Holocene palaeosols and aeolian activities in the Umimmalissuaq valley, West Greenland

Müller, Michael ; Thiel, Christine; Kühn, Peter

Published in:
The Holocene

Link to article, DOI:
10.1177/0959683616632885

Publication date:
2016

Document Version
Peer reviewed version

The Holocene

Holocene palaeosols and aeolian activities in the Umimmalissuaq valley, West Greenland

Journal:	*The Holocene*
Manuscript ID	HOL-15-0126.R1
Manuscript Type:	Paper
Date Submitted by the Author:	15-Dec-2015
Complete List of Authors:	Müller, Michael; University of Tübingen, Department of Geosciences, Institute of Geography, Chair of Soil Science and Geomorphology Thiel, Christine; Leibniz Institute for Applied Geophysics, Section 3: Geochronology and Isotope Hydrology Kühn, Peter; University of Tübingen, Department of Geosciences, Institute of Geography, Chair of Soil Science and Geomorphology
Keywords:	Palaeosols, aeolian transport, grain size analysis, AMS radiocarbon dating, deglaciation, Greenland, OSL dating
Abstract:	Aeolian sand sheets and active dunefields preserve an ancient Holocene land surface represented by palaeosols that occur around the present ice margin in the Kangerlussuaq area, West Greenland. To determine the relation between Holocene aeolian activities and periods of soil formation, both substantially dependent on the deglaciation history, palaeosols, aeolian sand sheets, and dunefields were analysed using field data, grain size analyses, optically stimulated luminescence dating and AMS ^{14}C data in an area of about 15 km² of the Ummimalissuaq valley. Located under dunefields close to the ice margin (< 2 km), palaeosols are developed in fine-grained aeolian sediment (silt loam) and covered by sandy aeolian layers. Silt contents of palaeosols of partly > 60 wt.% are comparable to aeolian sand sheets currently formed at further distances (4-5 km) from the present ice margin. We propose a transport distance of fine aeolian sediments, in which the palaeosols are formed, of at least 4 kilometres from inboard of the present ice margin. Soil formation of the palaeosols started around 2700 cal yr b2k. Datings from the youngest parts of the palaeosols suggest a stable period of around 2400 years, which allowed for pedogenesis and was characterised by low but constant aeolian activity. Since aeolian activity intensified after around 300 cal yr b2k and developed still active dunefields with coarse and medium sand accumulation, the ice margin must have reached its present position since then.

Holocene palaeosols and aeolian activities in the Umimmalissuaq valley, West Greenland

Michael Müller[1], Christine Thiel[2,3,4] and Peter Kühn[1]

[1] University of Tübingen, Department of Geoscience, Chair of Soil Science and Geomorphology, Rümelinstrasse 19-23, D-72070 Tübingen, Germany

[2] Leibniz Institute for Applied Geophysics, Section S3: Geochronology and Isotope Hydrology, Stilleweg 2, 30655 Hannover, Germany

[3] Nordic Laboratory for Luminescence Dating, Department of Geosciences, Aarhus University, Risø Campus, Frederiksborgvej 399, 4000 Roskilde, Denmark

[4] Centre for Nuclear Technologies (Nutech), Technical University of Denmark, Risø Campus, Frederiksborgvej 399, 4000 Roskilde, Denmark

Corresponding author:

Michael Müller, University of Tübingen, Department of Geoscience, Chair of Soil Science and Geomorphology, Rümelinstraße 19-23, D-72070 Tübingen, Germany

Email: michael.mueller@uni-tuebingen.de

Abstract

Aeolian sand sheets and active dunefields preserve an ancient Holocene land surface represented by palaeosols that occur around the present ice margin in the Kangerlussuaq area, West Greenland. To determine the relation between Holocene aeolian activities and periods of soil formation, both substantially dependent on the deglaciation history, palaeosols, aeolian sand sheets, and dunefields were analysed using field data, grain size analyses, optically stimulated luminescence dating and AMS ^{14}C data in an area of about 15 km^2 of the Ummimalissuaq valley. Located under dunefields close to the ice margin (< 2 km), palaeosols are developed in fine-grained aeolian sediment (silt loam) and covered by sandy aeolian layers. Silt contents of palaeosols of partly > 60 wt.% are comparable to aeolian sand sheets currently formed at further distances (4-5 km) from the present ice margin. We propose a transport distance of fine aeolian sediments, in which the palaeosols are formed, of at least 4 kilometres from inboard of the present ice margin. Soil formation of the palaeosols started around 2700 cal yr b2k. Datings from the youngest parts of the palaeosols suggest a stable period of around 2400 years, which allowed for pedogenesis and was characterised by low but constant aeolian activity. Since aeolian activity intensified after around 300 cal yr b2k and developed still active dunefields with coarse and medium sand accumulation, the ice margin must have reached its present position since then.

Keywords

Palaeosols, aeolian transport, grain size analysis, AMS radiocarbon dating, OSL dating, deglaciation, Greenland

Introduction

In general, areas close to the margins of ice sheets are strongly affected by aeolian activity (e.g. Dijkmans and Törnqvist, 1991; Willemse et al., 2003; French, 2007; Brookfield, 2011). This is mainly due to strong katabatic winds associated with steep pressure gradients that develop at the margins of ice sheets (Schaetzl and Loope, 2008; Brookfield, 2011), where they reach their highest speeds (Dijkmans and Törnqvist, 1991).

The driving controls on most aeolian systems and particularly on sand sheet environments like in West Greenland are the source area, the availability of the source material, and wind speed. The outwash-source zone for aeolian sand and silt is commonly controlled by variable discharge. In general, meltwater valleys near the margins of ice sheets are filled with silt-rich discharge in summer, and become dry and unprotected to aeolian erosion predominantly in winter (Schaetzl and Loope, 2008). Also, during winter with saltating snow and ice, aeolian mobility of sand is enhanced. The formation of a sand sheet either reflects adhesion to a wetted surface or with vegetation (e.g. Koster and Dijkmans, 1988; Ruz and Allard, 1995). Often, the presence of snow and interstitial ice binds aeolian particles to surfaces necessitating higher threshold shear velocities for transport (Ollerhead et al., 2013), though the sublimation rate may be an important factor in grain release (Van Dijk and Law, 1995). The presence of snow ramparts and interstitial layers mostly composed of snow can enhance aeolian accretion and dune movement (Koster and Dijkmans, 1988; Dijkmans and Mücher, 1989; Ruz and Allard, 1995). Further, aeolian transport and deposition of sand and silt is suggested to be affected and limited by topographical barriers (e.g. Mason et al., 1999; Mason, 2001).

Previous studies have shown a correlation between the distribution of wind-blown sediments and grain size, and the former extent of the ice sheet in West Greenland (e.g. Scholz and Grottenthaler, 1988; Dijkmans and Törnqvist, 1991; Willemse et al., 2003). Driven by Holocene climatic fluctuations alternating phases of both soil formation and aeolian activity occurred with different intensities (e.g. Stäblein, 1975; Ten Brink, 1975; Weidick, 1985;

Scholz and Grottenthaler, 1988; Dijkmans and Törnqvist, 1991; Van Tatenhove et al., 1996; Ozols, 2003; Willemse et al., 2003; Forman et al., 2007). The forefield of the inland ice margin was affected by permanent modifications of the palaeoenvironment due to changing glacial dynamics, and alternating glaciofluvial and aeolian processes. These processes may be linked in complex manners; however the intensity of glaciofluvial and aeolian processes decreases with increasing distance from the ice margin (Dijkmans and Törnqvist, 1991; Schaetzl and Loope, 2008), and correspondingly the influence of wind on erosion and sedimentation. Therefore, the changing distance from the ice margin to the outwash-source zone affected the variability in discharge, and thus the supply of aeolian sand and silt, which had impacts on the formation of soils, aeolian sand sheets and dunefields in the Holocene (cf. Willemse et al., 2003). Palaeosols developed in the aeolian sediments around Kangerlussuaq indicate an interruption or decrease of aeolian activity (e.g. Scholz and Grottenthaler, 1988; Dijkmans and Törnqvist, 1991; Willemse et al., 2003). They can be taken as proxies for stable environmental conditions. For the timing of soil formation different data exist. According to Van Tatenhove et al. (1996) soil formation in Sandflugtdalen (Figure 1a) north of the study area started around 4560 cal yr b2k. Willemse et al. (2003) assume an onset of soil formation prior to 3450 cal yr b2k and a halt in soil formation 600 cal yr b2k in Sandflugtdalen and Ørkendalen (Figure 1a). Similarly, Dijkmans and Törnqvist (1991) suggest soil formation between 3350 cal yr b2k and 650 cal yr b2k. Likewise, Forman et al. (2007) propose the beginning of soil formation after 3 ka, whereas Ozols (2003, 1600 cal yr b2k) and Scholz and Grottenthaler (1988, 1.5 ka) assume a distinct later start. In general, soil formation around Kangerlussuaq has been strongly connected to dynamics of the inland ice: During a retreat of ice, changing environmental conditions favoured soil formation in the study area due to lower discharge or more distal location from the source area, and thus lower intensity of katabatic winds and less supply of aeolian, whereas an advance led to an interruption of soil formation

caused by opposite conditions. However, knowledge regarding the exact timing of soil formation in the Kangerlussuaq area is still insufficient, and more data are needed.

In this study, we aim to characterise the results of interaction of both aeolian-geomorphic processes and pedogenic processes across an E-W oriented valley in West Greenland. We further aim to understand how the intensity of these processes changed in response to middle and late Holocene glacial retreat and readvance. The lines of evidence include 1) the spatial patterns of modern landforms, surface sediments, and soils, and 2) the stratigraphy observed along sampling transects, which allows for temporal reconstruction of these spatial patterns.

Study area

The Kangerlussuaq area is characterised by an E-W and ENE-WSW oriented valley system that leads the meltwater to the sea (Scholz and Grottenthaler, 1988). The E-W oriented Umimmalissuaq valley is located in West Greenland, around 30 kilometres southeast of Kangerlussuaq (Figures 1a, b).

Figure 1. (a) (b)

The bedrock in the study area is mainly Precambrian gneiss (e.g. Scholz and Grottenthaler, 1988; Ozols and Broll, 2003; Henriksen, 2008); therefore the aeolian transported material consists of non-calcareous and non-basaltic material. Based on own field observations, the Ørkendalen glacier (Figure 1b) at the eastern side of the study area forms an active moraine system, which is overrunning current vegetation (Figure 2a). We observed the meltwater to drain predominantly northward in the Ørkendalen valley, but also in the direction of the Umimmalissuaq valley. Forming a glacial outwash plain or sandur, and a delta, meltwater drains more or less directly into a lake system towards southwest and west, not using the Umimmalissuaq valley (Figures 1b, 2b). Compared to Sandflugtdalen or Ørkendalen, the

outwash plain is small (ca. 0.2 km²). The entire outwash plain generally acts as source for aeolian sediments. Own field observations indicated aeolian sand and silt to be mainly blown out from northwestern parts of the outwash plain (ca. 200-300 m southeast of profile D1, cf. Figure 1b), which are barely affected by meltwater channels in summer. Most parts of the valley itself are higher in elevation than the outwash plain (up to 50 m). The study area further includes the hills north and south of the valley, which rise up to 150 m higher than the outwash plain (Figures 1b, 2b).

The valley is covered by glacial deposits of the Keglen and Ørkendalen moraine systems as a result of the middle and late Holocene re-advances of the ice sheet (Stäblein, 1975; Ten Brink, 1975; Weidick, 1985). Moreover, glaciofluvial sediments are widespread in the valley. The glacial and glaciofluvial deposits, and most of the valley bottom and slopes are covered by a fine-grained aeolian sand sheet (ca. 60% coverage, Figure 1b), apart from areas close to the ice margin (sandur, recent moraine, dunefields). North, northwest and west of the glacial outwash plain, there are still active coarse-grained dunefields (ca. 5 % coverage; Figures 1b, 2b-d). Numerous distinct deflation areas cut into the aeolian sand sheet, and are present predominantly on top of moraines and slopes facing the ice margin (Figure 1b).

Figure 2. (a) (b) (c) (d)

The weather station closest to the study area is Kangerlussuaq Airport (Figure 1a). The present-day climate of Kangerlussuaq is Low Arctic continental: mean annual air temperature is -4.8°C and mean annual precipitation is 257 mm (1979-2008; according to data from Boas and Wang, 2011). Low precipitation in winter (Cappelen, 2001) indicates a thin snow cover in the study area during winter months (Ozols and Broll, 2003). In Kangerlussuaq, mean wind speed at 2 m above ground level is 3.6 m/s (1985-1999; Cappelen, 2001). Mean maximum wind speed at the same height is 19.6 m/s (1985-1999; Cappelen, 2001), and most frequent

wind direction is NE (Cappelen, 2001), indicating the effect of thermally induced katabatic winds and airflow channelling in the valleys (Van den Broeke and Gallée, 1996). The Umimmalissuaq valley is strongly affected by these katabatic winds which are stronger in winter due to a negative surface radiation and therefore a temperature deficiency above the snow-covered ablation zone (Willemse, 2000). Compared to Kangerlussuaq, the study area is linked directly to the inland ice (Figures 1a, b). Thus, it is most probably drier and colder, and more affected by high wind speeds due to a stronger influence of katabatic winds from the inland ice, which can be assumed of being active also during the Holocene.

The topographic position, the distance from the ice margin and the aspect seem to be mainly responsible for the type of vegetative cover, the soil distribution, and the thickness of the active layer of the permafrost in the study area. Permafrost exists at depths < 20-30 cm at north facing slopes, where organic-rich permafrost is common. At south facing slopes permafrost has not been detected < 1 m. North facing (moist) slopes have dense vegetation and organic-rich soil horizons within the active layer, whereas south facing (dry) slopes or ridges have little or no vegetation and are thus subject to deflation.

Materials and methods

Mapping and sedimentary analysis

The geomorphological map (Figure 1b) is based on aerial photographs of the Danish Geodetic Institute (scale 1:40 000; Kort and Matrikelstyrelsen, 1968), publications from Scholz and Grottenthaler (1988) and Ten Brink (1975), and own field surveys in 2009 and 2011.

In total 187 samples for grain size analysis (Supplementary material Table S1) were taken in dunefields north, northwest and west to the glacial outwash plain (Figures 1b, 2b-d), and in four cross-sections through the valley with different distances from the recent ice margin. Each cross-section comprises 9 resp. 10 sampling points; section 1 (sampling points 10-19) is distal (ca. 4-5 km) and section 4 (sampling points 40-48) proximal (ca. 2-3 km) to the ice

margin (Figure 1b). From each sampling point (10-48; Figure 1b) horizons at different depths were described according to the guideline for soil description (FAO, 2006) and subsequently sampled. At the cross-sections we refer to the upper 30 cm (maximum depth of active layer at north facing slopes) as the upper layer and to the horizons below 30 cm as the lower layer of the aeolian sand sheet, respectively.

Additional buried humic palaeosols (lower layer) - found under still active dunes (soil profiles D0-D3, Figure 1b) - were sampled. For the upper layer (layer above the palaeosol as described more detailed in Results) a soil texture hand test was done in field to determine bands of different grain sizes. The grain size distribution of all samples was determined in the laboratory after Blume et al. (2011) according to DIN ISO 11 277.

Furthermore, depth, width, length, inclination, and aspect of 16 selected deflation areas (Supplementary material Table S2) were measured to get an overview where deflation is active and which kind of material is subject to wind erosion.

Statistical analyses for grain size distribution patterns were implemented with the free programming language R, version 3.1.2 (R Development Core Team 2014) by applying R-packages *car* (Fox and Weisberg, 2011), and *RCMDR* (Fox, 2005).

Radiocarbon dating

Soil organic matter from the palaeosols was dated by AMS ^{14}C dating in the laboratory of Erlangen/Germany (abbr. Erl-; see Table 2). Calibration of ^{14}C data was done with OxCal 4.2 (Bronk Ramsey, 2009). Radiocarbon dating was performed on 14 samples after pre-treatment according to the acid-alkali-acid method: the samples were heated at 80°C in 1M HCl to remove carbonates. Then, the samples were heated at 80°C in 1M NaOH to remove humic acids and fulvic acids, respectively. Afterwards, the samples were heated at 80°C again in 1M HCl to remove remaining carbonates. Finally, the samples were dried at 100°C, and stored in closed glasses to avoid contamination. Six samples were taken from varying depths in profile

D1, and five samples from varying depths in profile D2 in the active dunefields (Figure 1b). Additionally, the soil organic matter of three palaesols of transects 1 to 3 were dated (profiles 17, 24, 33 in Figure 1b).

Optically stimulated luminescence dating

Four samples from profile D2 (sampling depths given in Table 3) were dated using both quartz and feldspar optically stimulated luminescence (OSL). Sand grains ranging from 90-180 µm were obtained through wet-sieving the bulk sample (taken in opaque tubes), followed by treatment with 10% HCl and 10% H_2O_2 and subsequent density separation using fast float (LST; potassium-rich feldspar $\rho < 2.58$ g cm^{-3}, quartz $\rho > 2.62$ g cm^{-3}). The mineral extracts were etched with 10% hydrofluoric acid (HF) for 30 minutes in case of feldspar, and with 40% HF for one hour in case of quartz, respectively. After etching, the samples were treated with 30% HCl in order to remove any fluorides which might have built during the treatment. Finally, the samples were washed with distilled water and dried at 50°C prior to re-sieving.

The purity of the quartz extracts was tested following Duller (2003). All samples were contaminated by feldspar, so the extracts were re-etched in 40% HF for 40 minutes, washed and re-sieved. The subsequent purity test showed that the aggressive treatment would not entirely remove the feldspar contribution to the OSL signal; thus this had to be done instrumentally.

The samples were measured using Risø TL/OSL readers (model DA-20; Thomsen et al. 2006) equipped with a calibrated $^{90}Sr/^{90}Y$ beta source and with both blue (470 nm) and infra-red (IR; 870 nm) emitting diodes. The luminescence signals of the quartz extracts were detected through a Hoya U-340 filter. Due to the feldspar contamination, the quartz was measured using a double single-aliquot regenerative (dSAR) protocol (Banerjee et al., 2001). To find suitable measurement settings, both a pre-heat plateau and thermal transfer were measured on sample 143080 (cf. Table 3) with preheat temperatures ranging from 160°C to 300°C. The

cut-heat temperature following a test dose of ~ 5 Gy was 20°C below the preheat temperature. For each setting three aliquots were used, and the mean equivalent dose (De) was calculated. Based on the results (Supplementary material Figure S1), a pre-heat of 200°C (cut-heat 180°C) was chosen. The pre-heat was followed by IR stimulation at 50°C (100 s) and a subsequent blue stimulation at 125°C (40 s). Each measurement cycle ended with a high temperature clean-out (280°C) using blue LEDs (40 s). For each sample, >30 small aliquots (few tens of grains) were measured. The initial 0.2 s of the decay curve minus a background from the subsequent 1 s was used for calculation. The OSL signals are dominated by the fast component (Supplementary material Figure S2); however, less than 1% of the aliquots passed the rejection criteria (recycling ratio within 10%, test dose error within 20%, signal more than 3 sigma above background). It was therefore decided to not continue the quartz measurements but test the feldspar extracts instead.

For equivalent dose measurements of the potassium-rich feldspar extracts, a single aliquot regenerative (SAR) procedure was employed (Wallinga et al., 2000) on small aliquots (few tens of grains). IR stimulation was carried out at 50°C for 100 s after preheating at 250°C (60 s); the response to the test dose of 2.5 Gy was measured in the same matter, followed by an IR clean-out at 280°C. The luminescence signal was detected through a Schott BG39/Corning 7-59 filter combination. For each sample, twelve aliquots were measured, and the mean De was calculated. The signal collected during the initial 1.6 s of stimulation minus a background from the last 40 s was used for calculation. All aliquots passed the rejection criteria (recycling ratio within 10%, test dose error within 10%, signal more than 3 sigma above background). Dose recovery tests were conducted in order to test whether a given dose (prior to any heating) can be accurately recovered. Three aliquots per sample were bleached for 4 hours in a Hönle SOL2 and then given a dose of 16 Gy (test dose 2.5 Gy) prior to measurement. For all samples except 143080, given doses of were recovered within 10% of unity, whilst for sample 143080, the recovery was only within 20% of unity.

As feldspar may suffer from anomalous fading (Wintle, 1973), which would result in an age underestimate, the fading rate (*g*-value) was measured on six aliquots per sample following Auclair et al. (2003). The same settings as for De determinations were used, and both several prompt measurements and delays up to 10 hours were included. The fading correction is based on Huntley and Lamothe (2001).

In order to determine the dose rate, the radionuclides (Table 3) were measured using high-resolution gamma-spectrometry (Murray et al., 1987). The radionuclide concentrations were converted into dose rates following Guérin et al. (2011), and the cosmic dose contribution was added (Prescott and Hutton, 1994).

Results

Aeolian deposits and landforms

Both small (< 50 cm height) and large (up to 2 m height) longitudinal dunes established particularly in the transition zone from the glacial outwash plain to the dunefields (next to profile D1, Figure 1b). The areas between these vegetated longitudinal dunes have no vegetative cover. In addition, dome-shaped and barchan-like dunes are present in the dunefields (Figure 2d); these become higher (>2 m) and larger with increasing distance from the glacial outwash plain. Aeolian sand ripples (e.g. Anderson, 1987; Yizhaq et al., 2004) are common both between and leeward of dunes, where steep sand ridges of several metres length and width were found: These sand ridges are characterised by the absence of vegetation (Figures 2c, d).

The depths of the aeolian sand sheet (Figure 1b) strongly depend on topographical features and the distance from the ice margin. Greater depths of 50 cm or even > 100 cm (Table S1) are found on wind-protected sites, e.g. in depressions and on leeward sides of moraines.

Deflation areas (Figure 1b) are widespread in the entire Umimmalissuaq valley and are mainly present on S-SE facing slopes or on crests and S-SE facing parts of moraines (Table S2). These often oval-shaped aeolian blow-outs are characterised by sparse or absent vegetative cover, and cut deep into the aeolian sand sheet. Often the underlying moraine material or bedrock is exposed by wind erosion. The size of deflation areas ranges from a few to hundreds of metres in width and length, as well as their depth that ranges from around 1 m next to the present dunefields (e.g. deflation area 13; Table S2; Figure 1b) to around 30 cm with increasing distance from the ice margin (e.g. 7, 9; Table S2; Figure 1b).

Sedimentary units and grain size distribution

All soil profiles in the large dunefield (represented by D1-D3, Figure 1b) show alternating sedimentary units of humus-free and humus-rich sediments. Buried humic palaeosols (Figure 3a: 1e-1g; Figure 3b: 2e-2h) can be taken as marker horizons dividing the profiles in an upper and a lower layer. The palaeosols are developed in the lower layer consisting mainly of fine sand and coarse silt (Figures 3a, b; for definition and contents of grain size fractions see Table S1). According to FAO (2006), the main texture of palaeosols is silt loam, sometimes sandy loam. The morphology of palaeosols visible in Figures 3c and 3d is characterised by a continuous horizontal to subhorizontal alternating stratification of buried Ah and C horizons with aeolian sand and silt. The centimeter to decimeter thick darker bands (Ah horizons) indicate organic matter accumulation, which are separated by millimeter to centimeter thick lighter bands (C horizons) of same soil texture (mostly silt loam). These bands feature a non-horizontal structure perturbed by cryoturbational processes (cf. Figures 3a-d). Palaeosols are covered by alternating bands (centimeter to decimeter) consisting of primarily coarse, medium and fine sand (upper layer; Figures 3a-d). The main texture in the upper layer is loamy coarse sand, but also sand is common, particularly in the uppermost bands. The clay content of < 5 wt.% is negligible. In general, dune profiles show an abrupt decline in coarse

and medium sand and an increase in fine sand and silt content at the transition from upper to lower layer (Figures 3a, b), reaching up to 64 wt.% silt in profile D3.

Figure 3. (a) (b) (c) (d)

The main texture of the aeolian sand sheet (Figure 1b), represented by cross-sections 1 to 4, is silt loam: silt and sand contents range between 25 and 75 wt.% (Table S1). The lower layer of the aeolian sand sheet reaches partly close to 100 % sand (Figures 4a, d). Clay content with a mean of 4 wt.% is negligible.

The majority of sampling points from cross-sections 1 to 3 show finer grain sizes in the upper layer (mostly silt loam; Table 1, Figures 4b, d) and coarser grain sizes in the lower layer (mostly sandy loam, partly sand; Table 1, Figures 4a, d), whereas cross-section 4 is still more affected by coarser grain sizes in the upper layer (partly loamy coarse sand; Table 1, Figures 4b, d). Within each cross-section the variability of grain sizes is very heterogeneous and is greater than between the respective cross-sections. Hereby, the variability of grain sizes in the upper layer of the cross-sections is distinctly lower and more homogeneous compared to the lower layer (Table 1, Figure 4d).

Table 1.

In general, sand contents significantly decrease with increasing distance from the ice margin (Pearson $r = -0.29$, $p < 0.001$), whereas silt contents increase ($r = 0.27$, $p < 0.001$). This is even more pronounced in the upper layers of dune profiles and sampling points (sand: $r = -0.69$, $p < 0.001$; silt: $r = 0.68$, $p < 0.001$; Figure 4e). However, the lower layers do not show a significant decline in grain sizes with increasing distance from the ice margin (sand: $r = 0.09$, $p = 0.40$; silt: $r = -0.13$, $p = 0.25$; Figures 4a, d).

Grain sizes in the lower layer of dune sediments (palaeosols) are similar to grain sizes in the upper layer of cross-sections (texture: silt loam; Figures 4c, d; Table 1). A Levene test revealed variance homogeneity between palaeosols (lower layer) and the upper layers of cross-sections 1 to 4 ($F = 0.23$, $p = 0.92$). Using ANOVA ($F = 1.51$, $p = 0.20$) and following Post-hoc Tukey test, we found no significant differences between grain sizes of palaeosols and cross-section 1 ($p = 0.54$), cross-section 2 ($p = 0.30$), cross-section 3 ($p = 0.94$), and cross-section 4 ($p = 0.99$). The grain sizes in upper layers of cross-sections 1 and 2, and cross-sections 3 and 4, respectively, are similar.

Figure 4. (a) (b) (c) (d) (e)

AMS ^{14}C ages

A summary of AMS ^{14}C ages is given in Table 2. Soil organic matter from the palaeosol of profile D1 (Figure 3a) was dated to 330-57 cal yr b2k at a depth of 85 cm (Erl-19002), to 1113-848 cal yr b2k at 95 cm (Erl-16621), and to 2731-2209 cal yr b2k at 140 cm (Erl-19003). The palaeosol of profile D2 (Figure 3b) yields ages of 110-92 cal yr b2k in 76 cm depth (Erl-16622), 2975-2795 cal yr b2k in 115 cm depth (Erl-16623), and 2749-2258 cal yr b2k in 140 cm depth (Erl-19004).

Samples taken from the cover sediments of the palaeosols and the transition zone between cover sediments and palaeosols show very young and imprecise ages (Erl-16619, Erl-16620, Erl-16622, Erl-19002), caused by organic matter, which has been developed during the atomic age since 1945.

Additionally, soil organic matter of buried palaeosols within cross-sections 1 to 4 was analysed. Sampling point 17 (Figures 1b, 5a) reveals an AMS ^{14}C age of 5335-4919 cal yr b2k (Erl-19000); this is so far the oldest age of soil organic matter from the valley bottom. A palaeosol from sampling point 33 (Figures 1b, 5c) has an AMS ^{14}C age of 4876-4499 cal yr

b2k (Erl-16614). Soil organic matter from sampling point 24 (Figures 1b, 5b) was AMS ^{14}C dated to 2975-2800 cal yr b2k (Erl-19001).

Table 2.

Luminescence ages

The total dose rates to feldspar taken from profile D2 vary between 2.04 ± 0.07 Gy/ka (sample 143081; cf. Table 3) and 2.37 ± 0.08 Gy/ka (sample 143078). The equivalent doses (D_e values) are more variable: The largest D_e of 12.8 ± 0.8 Gy was observed for sample 143079 (D2-53), and the smallest (2.4 ± 0.1 Gy) for sample 143080). The IRSL ages given are all fading corrected; the *g*-values vary between 2.87 ± 0.03 %/decade (143080) and 3.81 ± 0.17 %/decade (143078). In palaeosol D2, the uppermost sample (20 cm depth) was dated to 2.2 ± 0.1 ka, while the sample at a depth of 53 cm (143079) has an IRSL age of 7.3 ± 0.6 ka. Sample 143080, just 16 cm below sample 143079, was dated to 1.4 ± 0.1 ka, whilst the lowermost sample (143081) at a depth of 115 cm resulted in 3.7 ± 0.2 ka.

It is apparent that age inversions are present, i.e. the upper horizons show older ages than the lower ones. A possible cause for this might be age overestimation of the upper layers due to incomplete luminescence signal re-setting while the grains were being transported. The higher sand content of these two samples implies a shorter distance to the ice margin, which can result in poorer signal re-setting (e.g. Alexanderson and Murray, 2012). Further, it is possible that the material was mainly transported during winter months; in this case the sand will not have seen much daylight prior to its deposition. However, it is also possible that the ages of the lower samples are erroneous (dose recovery of sample 143080 was poor). A greater set of samples will be needed to investigate these issues in detail. Further, as the quartz OSL did not give any results to compare the IRSL ages with, we reject the OSL data for any further discussion but do point out that there is partial agreement with the AMS ^{14}C data (see below).

Table 3.

Figure 5. (a) (b) (c)

Discussion

Linking aeolian processes and palaeosols

The main requirements for aeolian transport of sand and silt across the Umimmalissuaq valley are (i) sufficient supply of coarse-grained and fine-grained material from the glacial outwash plain and (ii) the frequently blowing katabatic winds combined with (iii) the peculiar arid climate conditions at the ice margin (cf. Bullard and Austin, 2011).

Coarse-grained material (predominantly medium sand and coarse sand, upper layer; Figures 3a, b, 4b; Table S1) is deposited predominantly in the active dunefields (Figure 1b) north, northwest and west of the glacial outwash plain. Scholz and Grottenthaler (1988) propose that, with the exception of active dunefields, no recent accumulation of aeolian material takes place in the study area. However, dust clouds have been observed to rise up to several hundreds of meters in the study area during summer. Even ice-near areas are covered by a thin layer of fine sand and silt after such events (cf. German, 1971; Willemse et al., 2003). This may also currently provide durable (if combined with rainfall) sedimentation of fine sand and silt (upper layer of cross-sections in Figures 4b, d, e) in most parts of the Umimmalissuaq valley. Most likely, these events are stronger in winter because of a higher wind drift potential during this time of the year (e.g. Willemse, 2000), and the outwash-source zone is dry and unprotected against aeolian erosion (Schaetzl and Loope, 2008).

Deflation areas are widespread in the study area (Figure 1b), also in active dunefields. These deflation areas occur in the older aeolian sand sheet consisting of fine material, and hereby predominantly on wind exposed S-SE slopes and moraines with depths up to 1 m and areas

from a few up to hundreds of m² (Table 5). Similarly, Dijkmans and Törnqvist (1991) describe a SE-NW orientation of these often bowl-shaped or oval-shaped aeolian blow-outs, sometimes up to 1 m deep with diameters of up to several tens of meters (cf. French, 2007). These frequently occurring blow-outs imply reworking of previously deposited sand and silt by wind, and wind erosion as the prevailing aeolian process outside the dunefields.

Within the active dunefields 1-2 km from the ice margin (Figure 1b), humic palaeosols (lower layer, consisting of silt loam, Figures 3a, b) are developed in older sand sheets and preserved by deposition of the dune sands above (upper layer, consisting of loamy sand, Figures 3a, b). Generally, (i) the proportion of finer grain sizes (clay, silt) in the dunefields with < 15 wt.% is very small, (ii) the underlying cumulic palaeosols with finer material have no layers with coarser material comparable to the overlying dunes. According to Ten Brink (1975) the palaeosols are located within the Ørkendalen moraine system (Figure 1b). Hence, the lower layer, in which the palaeosols have formed, must have accumulated after the formation of the Ørkendalen moraines, since the lower layer is clearly not of glacial origin. At that time, the ice had disappeared and a decreasing influence of the strong and dry katabatic winds affected moisture conditions and thus the availability of sediments, soil formation and correspondingly vegetation in the valley. Further, the dominance of pedogenesis after the formation of the Ørkendalen moraines reflects a balance between pedogenesis and the sedimentation rate, i.e. the cumulic palaeosols (with grain sizes predominantly of fine sand and coarse silt, Figures 3a-d) of more than 60 cm thickness represent a phase with lower intensity of aeolian activity and synsedimentary pedogenesis. During that period of time, the sedimentation rate generally and particularly of coarse-grained material (sand) decreased which favoured pedogenic processes. However, thin lighter layers between thicker organic rich layers within the buried Ah horizons suggest intermittent sedimentation events during soil formation. These observations indicate that there was an episodically easily available source of fine to medium sand in the source area, and quickly colonising sedges and other vascular plants in the

sedimentation area. Thus, pedogenesis became more intense during periods with decreasing sedimentation rates and vice versa. It is important to notice that the soil formation after the formation of the Ørkendalen moraines does not reflect an on-off system of aeolian sedimentation. Instead, alternating periods of enhanced and weaker soil formation occurred depending on the sedimentation rate. Cryoturbation features in the palaeosols of show the soil horizons of palaeosols D1 and D2 (Figures 3a-d) were partly subject to cryoturbation and alternating of frost-thaw processes during the period of soil formation. This has to be also taken into account when interpreting any dating ages.

Since the ages from the lower boundaries of the palaeosols above the permafrost date back to 2731-2209 cal yr b2k (D1, 140 cm, Figure 3a) and 2749-2258 cal yr b2k (D2, 140 cm, Figure 3b), and the ages of the upper parts of the palaeosols date back to 330-57 cal yr b2k (D1, 85 cm, Figure 3a) and 110-92 cal yr b2k (D2, 76 cm, Figure 3b), a period of at least 2400 years of relatively stable conditions related to pedogenesis is very likely. Interestingly, we found with 2975-2795 cal yr b2k in 115 cm of profile D2 an older age than in 140 cm (Figure 3b). This inversion of ages may reflect a rejuvenation effect, which is likely caused by an accumulation of younger humic substances above the permafrost table. A reason for that may be also cryoturbation processes, which led to relocation of soil organic matter (Bockheim, 2007).

A sample from the oldest parts of a palaeosol in the Umimmalissuaq valley yielded a relatively young TL (Thermoluminescence) age indicating the onset of soil formation after the Ørkendalen period around 1380-980 ka (Scholz and Grottenthaler, 1988). Even though little information is provided on the TL data, one has to assume an age underestimate as anomalous fading has not been taken into account at that time. Ages from palaeosols in Sandflugtdalen indicate a distinct earlier beginning of soil formation around 4680-4490 cal yr b2k (UtC-2034, Van Tatenhove et al., 1996). Our data for the start of soil formation are similar to 3869-3123 cal yr b2k (UtC-5624; Willemse et al., 2003), to 3442-3263 cal yr b2k (GrN-14655; Dijkmans

and Törnqvist, 1991), and to 3.19-2.67 ka (UIC-1556) and 3.16-2.69 ka (UIC-1558; Forman et al., 2007; all from Sandflugtdalen and Ørkendalen, respectively). Two buried organic layers in Sandflugtdalen, which indicate the onset of soil formation, reveal younger ages of 1941-1236 cal yr b2k and 1866-1232 cal yr b2k (Ozols, 2003). The results from the Umimmalissuaq valley indicate an earlier start of soil formation than discussed above. This may be confirmed in the future, since the base of the organic rich permafrost was not reached in profiles D1 and D2 in 2011. The lowermost AMS ^{14}C ages are from top of the permafrost table.

In the study area, aeolian activity intensified after around 300 cal yr b2k (Erl-16620, Erl-19002, Table 2), and medium to coarse sand (Figures 3a, b) was transported from a nearby available source forming dunefields (upper layer), which cover the palaeosols in the foreland of the active ice margin. This suggests a markedly increasing sedimentation rate of coarse-grained material. Most likely, these processes have been caused by a close ice margin followed by stronger dry katabatic winds and changes in sediment supply when the formation of the dunefields began. This would explain also the distinct coarser grain sizes compared to the lower layer. The more or less continuous redistribution (erosion and accumulation) of predominantly coarse-grained sand by intensive and prevailing aeolian activity in the area of the dunefields limited further soil formation since then. Despite landscape heterogeneity in the study area, only the outwash plain and the adjacent terminal moraines (ice-cored moraines) can be the present sediment source (Figure 1b).

All these findings lead us to the assumption that the sedimentation of the coarse material in the dunefields is connected to an advancing ice margin and its sandur area (if present), representing the source of the coarse material. This means additionally that a period of time with predominant deposition of fine material is most likely related to a more easterly situated ice margin, because the lacking of coarse material in the lower layer of dunefields.

Compared to our results, a (re)accumulation of aeolian sand after the period of soil formation in Ørkendalen and Sandflugtdalen is assumed to have started earlier around 595-550 cal yr b2k (UtC-5619; Willemse et al., 2003), and 735-560 cal yr b2k (GrN-14651; Dijkmans and Törnqvist, 1991; for further data see Table 2). The different timings of the sedimentation of wind-blown coarser material could be interpreted related to the ice margin in the way, that the Late Holocene advance of the ice reached the present ice margin in the Umimmalissuaq valley later than in northerly adjacent valleys.

Implications for the deglaciation history of the Umimmalissuaq valley

The ice margin in West Greenland in general is assumed to have reached its present position already around 6000 yr BP, followed by a minimum extent behind the present ice margin at around 4000 yr BP during the Holocene thermal maximum (Ten Brink and Weidick, 1974; Simpson et al., 2009). Since that time the ice sheet advanced again to its recent limits and further, resulting in younger moraine deposits (e.g. Ørkendalen, Figure 1b). Several different data exist for the Ørkendalen moraine system in West Greenland: it has been dated to 700-300 BP (Ten Brink, 1975; UW-180, Table 2) and to 2.5-1.5 ka (Scholz and Grottenthaler, 1988). In great contrast, other studies date the Ørkendalen moraine system to 6.8 ± 0.3 ka by ^{10}Be (Levy et al., 2012) and to 6.8 ± 0.3 cal ka b2k (UtC-1987, UtC-1990; Van Tatenhove et al., 1996; Table 2).

In contrast, our AMS ^{14}C data from soil organic matter of the overlying palaeosols in the Umimmalissuaq valley yielded a minimum age of 2749-2258 cal yr b2k (Erl-19004, Table 2) for the Ørkendalen moraines, most likely even older (cf. 2975-2795 cal yr b2k, Erl-16623). Our data are in line with the proposed 3450 cal yr b2k (UtC-5624; Willemse et al., 2003) and 3350 cal yr b2k (GrN-14655; Dijkmans and Törnqvist, 1991) for the recession of the ice margin in Sandflugtdalen and Ørkendalen. After development of the Ørkendalen moraines the inland ice melted again at its margin and retreated beyond its present limit. Previous studies

proposed a former recession of the ice margin in West Greenland after formation of the Ørkendalen moraines of more than 10 kilometres (Weidick, 1985; Scholz and Grottenthaler, 1988), or even of 16 kilometres (Van Tatenhove et al., 1996). The changing distance from the ice margin to the outwash-source zone after formation of the Ørkendalen moraines affected the formation of soils, aeolian sand sheets and dunefields in the study area (cf. Willemse et al., 2003). Since grain sizes decrease significantly with increasing distance from the ice margin (Figure 4e), and since grain sizes and their variability within the upper layer of cross-section 1 (silt contents: 54 ± 6 wt.%; Table 1, Figures 4c, d) 4-5 km west of the present ice margin are comparable to palaeosols covered by coarse-grained dunes (silt contents: 49 ± 9 wt.%; Table 1, Figures 4c, d), we propose a transport distance of the fine aeolian sediments, in which the palaeosols have formed, of < 4 kilometres from inboard of the present ice margin.

AMS ^{14}C ages of 5335-4919 cal yr b2k (sampling point 17), 4876-4499 cal yr b2k (33), and 2975-2800 cal yr b2k (24) (Figure 1b, Table 2) indicate soil formation also before 2749-2258 cal yr b2k (Erl-19004; Table 2). These palaeosols are situated between 4 and 5 km away from the present ice margin. All sampling points are located within the Umîvît/Keglen moraines (according to Ten Brink, 1975). This further implies a recession of the ice margin between the Umîvît/Keglen stage (with 7300 cal yr b2k, UtC-1987, UtC-1990, after Van Tatenhove et al., 1996, Table 2) and the Ørkendalen stage at least around 2700 cal yr b2k (Erl-19004; Table 2). As a consequence of lacking additional luminescence or ^{10}Be ages from the glacial sediments in the Umimmalissuaq valley the precise boundary between Umîvît/Keglen and Ørkendalen moraines is not clear.

Conclusions

During the Holocene the Umimmalissuaq valley has strongly been influenced by aeolian activities. This valley has a characteristic east-west orientation like numerous other valleys in

West Greenland, and herewith the observed phenomena can be generally taken as representative for other valleys close to the ice margin in West Greenland.

Currently deflation – predominantly caused by easterly katabatic winds – redistributes aeolian sand sheets (silt loam) further west and forms active dunefields (consisting of loamy coarse sand and sand). Active dunefields occur particularly at south facing slopes north, northwest and west to the glacial outwash plain within around 2 km of the present ice margin. The data of grain size distribution, and AMS ^{14}C data of the soils in the Umimmalissuaq valley lead to the following findings:

1. Aeolian activity intensified after around 300 cal yr b2k and the still active dunefields with coarse and medium sand accumulation (upper layer) developed. Thus we infer the ice margin must have reached its present position around 300 cal yr b2k.
2. Palaeosols with humic A horizons located within the Ørkendalen moraine system are developed in fine-grained aeolian sediment (silt loam - lower layer). They are covered by coarse-grained aeolian bands (loamy coarse sand to sand - upper layer). The lower layer, in which the palaeosols have formed, shows grain sizes comparable to aeolian sand sheets (upper layer), which are currently formed distal (in around 4 km distance) to the ice margin. Thus, we assume a transport distance of the fine aeolian sediments of the lower layer – buried under the present dunefield next to the ice margin – of at least 4 kilometres from inboard of the present ice margin.
3. AMS ^{14}C dating of soil organic matter of these buried palaeosols yielded a minimum age of 2749-2258 cal yr b2k for the start of soil formation. Since traces of moraine material overlying the palaeosols could not be detected, this particular area must have been ice-free since that time. A potential earlier start of soil formation may be confirmed in the future, since the base of the organic rich permafrost was not achieved in profiles D1 and D2 in 2011. In contrast, the lowermost AMS ^{14}C ages from palaeosols buried under the dunefield are from top of the permafrost table.

4. According to the youngest AMS ^{14}C ages of the buried palaeosols a stable period of at least 2400 years can be inferred during the Late Holocene, in which the area was characterised by pedogenesis and low intensity of aeolian activity, but with constant input of fine sand and silt (lower layer).

Acknowledgements

This study was partly funded by DAAD (German Academic Exchange Service) and the Gesellschaft für Erd- und Völkerkunde in Stuttgart. The first author would also like to thank Christian Wolf and Jürgen Förth for their assistance during fieldwork and the great time in Greenland. The last author thanks all students helping in the field, and Frank Baumann, Joachim Eberle, Jessica Henkner, and Thomas Scholten for fruitful discussions.

References

Alexanderson H and Murray AS (2012) Luminescence signals from modern sediments in a glaciated bay, NW Svalbard. *Quaternary Geochronology* 10: 250-256.

Anderson RS (1987) A theoretical model for aeolian impact ripples. *Sedimentology* 34: 943-956.

Auclair M, Lamothe M and Huot S (2003) Measurement of anomalous fading for feldspar IRSL using SAR. *Radiation Measurements* 37: 487–492.

Banerjee D, Murray AS, Bøtter-Jensen L, Lang A (2001) Equivalent dose determination from a single aliquot of polymineral fine grains. *Radiation Measurements* 33: 73-94.

Blume HP, Stahr K and Leinweber P (2011) *Bodenkundliches Praktikum: Eine Einführung in pedologisches Arbeiten für Ökologen, insbesondere Land- und Forstwirte, und für Geowissenschaftler*. 3. Aufl.. Spektrum Akademischer Verlag, Heidelberg.

Boas L and Wang PR (2011) *Weather and climate data from Greenland 1958-2010*. Observation data with description. DMI Technical Report 11-15. Danish Meteorological Institute. Copenhagen.

Bockheim JG (2007) Importance of cryoturbation in redistributing organic carbon in permafrost-affected soils. *Soil Science Society of America Journal* 71(4): 1335. doi:10.2136/sssaj2006.0414N.

Bronk Ramsey C (2009) Bayesian analysis of radiocarbon dates. *Radiocarbon* 51(1): 337-360.

Brookfield ME (2011) Aeolian processes and features in cool climates. In: Martini IP, French HM, Perez Alberti A (eds) *Ice-marginal and Periglacial Processes and Sediments*. Geological Society, London, Special Publications 354: 241-258.

Bullard JE and Austin MJ (2011) Dust generation on a proglacial floodplain, West Greenland. *Aeolian Research* 3: 43-54.

Cappelen J, Jørgensen BV, Laursen EV, Stannius LS, Thomsen RS (2001) *The Observed Climate of Greenland, 1958-99 – with Climatological Standard Normals, 1961-90*. DMI Technical Report 00-18, Copenhagen.

Dijkmans JWA and Mücher HJ (1989) Niveo-aeolian sedimentation of loess and sand: an experimental and micromorphological approach. *Earth Surface Processes and Landforms* 14: 303-315.

Dijkmans JWA (1990) Niveo-aeolian sedimentation and resulting sedimentary structures; søndre strømfjord area, Western Greenland. *Permafrost Periglacial Processes* 1: 83-96.

Dijkmans JWA and Törnqvist TE (1991) Modern periglacial eolian deposits and landforms in the Søndre Strømfjord area, West Greenland and their palaeoenvironmental implications. *Meddelelser øm Grønland, Geosciences* 25: 1-39.

Duller GAT (2003) Distinguishing quartz and feldspar in single grain luminescence measurements. *Radiation Measurements* 37: 161-165.

Food and Agriculture Organisation of the United Nations (FAO), 2006. Guideline for soil description. 4th ed. Rome.

Forman SL, Marin L, Van der Veen C, Tremper C, Csatho B (2007) Little Ice Age and neoglacial landforms at the Inland Ice margin, Isunguata Sermia, Kangerlussuaq, west Greenland. *Boreas* 36: 341-351.

Fox J (2005) The R Commander: A basic-statistics graphical user interface to R. *Journal of Statistical Software* 14(9): 1-42.

Fox J and Weisberg S (2011) An R companion to applied regression. 2nd edition, Sage. 472 pp. URL: http://socserv.socsci.mcmaster.ca/jfox/Books/Companion

French HM (2007) *The periglacial environment*, third ed. John Wiley and Sons Ltd, Chichester.

German R (1971) Die wichtigsten Sedimente am Rande des Eises – ein aktuogeologischer Bericht von der Stirn des Kiagtutsermia bei Narssarssuaq (Süd-Grönland). *N. Jb. Geol. Paläont.* 138: 1-14.

Guérin G, Mercier N and Adamiec G (2011) Dose-rate conversion factors: update. *Ancient TL* 29 (1): 5-8.

Henriksen N (2008) *Geological history of Greenland*. Geological Survey of Denmark and Greenland (GEUS). Copenhagen.

Huntley DJ and Lamothe M (2001) Ubiquity of anomalous fading in K-feldspars and the measurement and correction for it in optical dating. *Canadian Journal of Earth Sciences* 38: 1093–1106.

Kort and Matrikelstyrelsen (former Danish Geodetic Institute) (1968) *Aerial images of Greenland*. Copenhagen.

Koster EA and Dijkmans JWA (1988) Niveo-aeolian deposits and denivation forms, with special reference to the Great Kobuk sand dunes, Northwestern Alaska. *Earth Surface Processes and Landforms* 13: 153-170.

Levy LB, Kelly MA, Howley JA, Virginia RA (2012) Age of the Ørkendalen moraines, Kangerlussuaq, Greenland: constraints on the extent of the southwestern margin of the Greenland Ice Sheet during the Holocene. *Quat. Sci. Rev.* 52: 1-5.

Mason JA (2001) Transport direction of Peoria loess in Nebraska and implications for loess source areas on the central Great Plains. *Quaternary Research* 56: 79-86.

Mason JA, Nater EA, Zanner CW, Bell JC (1999) A new model of topographic effects on the distribution of loess. *Geomorphology* 28: 223-236.

Murray AS, Marten R, Johnston A, Martin P (1987) Analysis for naturally occurring radionuclides at environmental concentrations by gamma spectrometry. *Journal of Radioanalytical and Nuclear Chemistry* 115: 263-288.

Ollerhead J, Davidson-Arnott R, Walker IJ, Matthew S (2013) Annual to decadal morphodynamics of the foredune system at Greenwich Dunes, Prince Edward Island, Canada. *Earth Surface Processes and Landforms* 38: 284-298.

Ozols U (2003) Bodenökologische Prozesse in permafrostbeeinflussten Böden Westgrönlands. Vergleich von *Kobresia myosuroides*-, *Salix glauca*- und *Betula nana*-Beständen. Band 13, Arbeiten aus dem Institut für Landschaftsökologie Westfälische Wilhelms-Universität Münster.

Ozols U and Broll G (2003) Soil ecological processes in vegetation patches of well drained permafrost affected sites (Kangerlussuaq – Greenland). *Polarforschung* 73(1): 5-14.

Prescott JR and Hutton JT (1994) Cosmic ray contributions to dose rates for luminescence and ESR dating: large depths and long-term variations. *Radiation Measurements* 23: 497-500.

R Development Core Team (2014) R: A language and environment for statistical computing. R Foundation for Statistical Computing, Vienna, Austria. http://www.R-project.org/ (accessed 02 June 2015).

Ruz MH and Allard M (1995) Sedimentary structures of cold-climate coastal dunes, Eastern Hudson Bay, Canada. *Sedimentology* 42: 725-734.

Schaetzl RJ and Loope WL (2008) Evidence for an aeolian origin for the silt-enriched soil mantles on the glaciated uplands of eastern Upper Michigan, USA. *Geomorphology* 100: 285-295.

Scholz H and Grottenthaler W (1988) Beiträge zur jungholozänen Deglaziationsgeschichte im mittleren Westgrönland. *Polarforschung* 58(1): 25-40.

Simpson MJR, Milne GA, Huybrechts P, Long AJ (2009) Calibrating a glaciological model of the Greenland ice sheet from the Last Glacial Maximum to present-day using field observations of relative sea level and ice extent. *Quat. Sci. Rev.* 28: 1631-1657.

Stäblein G (1975) Eisrandlagen und Küstenentwicklung in West-Grönland. *Polarforschung* 45(2): 71-86.

Storms JEA, de Winter IL, Overeem I, Drijkonigen GG, Lykke-Andersen H (2012) The Holocene sedimentary history of the Kangerlussuaq Fjord-valley fill, West Greenland. *Quat. Sci. Rev.* 35: 29-50.

Ten Brink NW (1975) Holocene history of the Greenland ice sheet based on radiocarbon-dated moraines in West Greenland. *Meddelelser øm Grønland* 201(4): 1-44.

Ten Brink NW and Weidick A (1974) Greenland ice sheet history since the last glaciation. *Quaternary Research* 4: 429-440.

Thomsen KJ, Bøtter-Jensen L, Denby PM, Moska P, Murray AS (2006) Developments in luminescence measurement techniques. *Radiation Measurements* 41: 768-773.

Van den Broeke MR and Gallée H (1996) Observation and simulation of barrier winds at the western margin of the Greenland ice sheet. *Q. J. R. Meteorolog. Soc.* 122: 1365-1383.

Van Dijk D and Law J (1995) Sublimation and aeolian sand movement from a frozen surface: experimental results from Presqu'ile Beach, Ontario. *Geomorphology* 11: 177-187.

Van Tatenhove FGM, Van der Meer JJM and Koster EA (1995) Implications for deglaciation chronology from new AMS age determinations in Central West Greenland. *Quat. Res.* 45: 245-253.

Wallinga J, Murray A and Duller G (2000) Underestimation of equivalent dose in single-aliquot optical dating of feldspars caused by preheating. *Radiation Measurements* 32: 691–695.

Weidick A (1985) Review of glacier changes in West Greenland. *Z. Gletscherkd. Glazialgeol.* 21: 301-309.

Willemse NW, Koster EA, Hoogakker B, Van Tatenhove FGM (2003) A continuous record of Holocene eolian activity in West Greenland. *Quat. Res.* 59: 322-334.

Willemse NW (2000) Arctic Natural Archives, lake and eolian sedimentary records from West Greenland.Netherlands Geographical Studies 272. Utrecht.

Wintle AG (1973) Anomalous fading of thermoluminescence in mineral samples. *Nature* 245: 143-144.

Yizhaq H, Balmforth NJ and Provenzale A (2004) Blown by wind: nonlinear dynamics of aeolian sand ripples. *Physica D* 195: 207–228.

Tables

Table 1. Variability of grain sizes (data shown in wt.%) in dune sediments and the respective cross-sections; SD = standard deviation.

Table 2. AMS ^{14}C data and luminescence data of samples related to glacial, glaciofluvial and aeolian deposits in the Kangerlussuaq area, West Greenland, classified in the chronological context.

Table 3. Luminescence dating information, including radionuclide concentrations, water contents, dose rates (Dr), equivalent doses (De), g-values (i.e. fading rates) and (fading corrected) ages. Preference is given to the fading corrected ages. See text for details. n = number of aliquots measured to obtain average De's; s.e. = standard error.

Figures

Figure 1. (a) Map of the area around Kangerlussuaq, West Greenland showing the study area and the adjacent valleys Sandflugtdalen and Ørkendalen; modified after Storms et al., 2012. (b) Geomorphological map of the Umimmalissuaq valley based upon air-photo interpretation, field evidence, and additional information in Ten Brink (1975).

Figure 2. (a) Recent moraine of Ørkendalen glacier overrunning current vegetation. Photo (2014) was taken towards northwest. (b) Umimmalissuaq valley with the glacial outwash plain and the large dunefield west/northwest of the outwash plain (for locations see Figure 1b) - taken towards west/northwest. (c), (d) Large dunefield, glacial outwash plain and Ørkendalen glacier - (c) taken from profile D3 towards east, (d) taken from profile D2 towards east.

Figure 3. Dune profiles D1 and D2 (for location see Figure 1b) showing buried humic palaeosols and overlying dune sands. (a), (b) Profile sketches of D1 and D2 with AMS ^{14}C data of soil organic matter, IRSL data, grain size distribution and pedology. For unmarked bands a soil texture hand test was done in field. The darker the palaeosol the higher the amount of soil organic matter. In both profiles permafrost was detected below 140 cm. (c), (d) Photos of profiles D1 and D2 showing palaeosols (lower layer) and overlying dune sands (upper layer). Traces of cryoturbation are present in both palaeosols.

Figure 4. (a), (b), (c) Soil texture ternary diagrams (data shown in wt.%). (a) Lower layer of cross-sections 1 to 4 compared to lower layer of dunefields. Dune profiles show relatively fine, the sampling points from cross-section 1 to 4 partly coarse grain sizes. (b) Upper layer of cross-sections 1 to 4 compared to the upper layer of dunefields. Highest sand contents,

particularly in both coarse and medium sand range, were found in the dunefields. Cross-section 4 has higher contents of sandy loam compared to cross-sections 1 to 3. (c) Lower layer of dunefields compared to the upper layer of cross-section 1. Note that grain sizes from the lower layer of dune profiles are in the same range as from the upper layer of cross-section 1. (d) Variability of sand content (wt.%) in the upper layer (UL) and lower layer (LL) of dune sediments (Dunes) and cross-sections 1 to 4 (C1, C2, C3, C4). (e) Mean sand content (wt.%) in the upper layer of dune sediments (filled dots) and cross-sections 1 to 4 (blank dots) with increasing distance (m) from the ice margin.

Figure 5. Selected soil profiles from cross-sections showing grain size distribution, pedology and AMS ^{14}C data of soil organic matter. (a) Profile 17 (cross-section 1). (b) Profile 24 (cross-section 2). (c) Profile 33 (cross-section 3). For location of soil profiles see Figure 1b.

Supplementary material

Table S1. Grain size analysis of all soil samples. Abbreviations and grain size fractions: cS = coarse sand (0.63-2 mm), mS = medium sand (0.2-0.63 mm), fS/ffS = fine sand/very fine sand (fS: 0.125-0.2 mm, ffS: 0.063-0.125 mm), cU = coarse silt (0.02-0.063 mm), mU = medium silt (0.0063-0.02 mm), fU = fine silt (0.002-0.0063 mm), clay (< 0.002 mm). For location of soil profiles see Figure 1b.

Table S2. Investigated deflation areas illustrating measured aspects, inclinations, widths, lengths and depths. Description of aspect: S=South, SE=Southeast. The aspect and inclination are related to the hosting slope and moraine. The locations of the investigated deflation areas are shown in Figure 1b with *italic numbers*.

Figure S1. OSL preheat plateau and thermal transfer for sample 143080. A preheat temperature of 200°C was chosen for the measurements.

Figure S2. a) Natural and b) regenerated (7 Gy) quartz OSL decay curve of one aliquot of sample 143079. The fast decay implies the presence of the fast component.

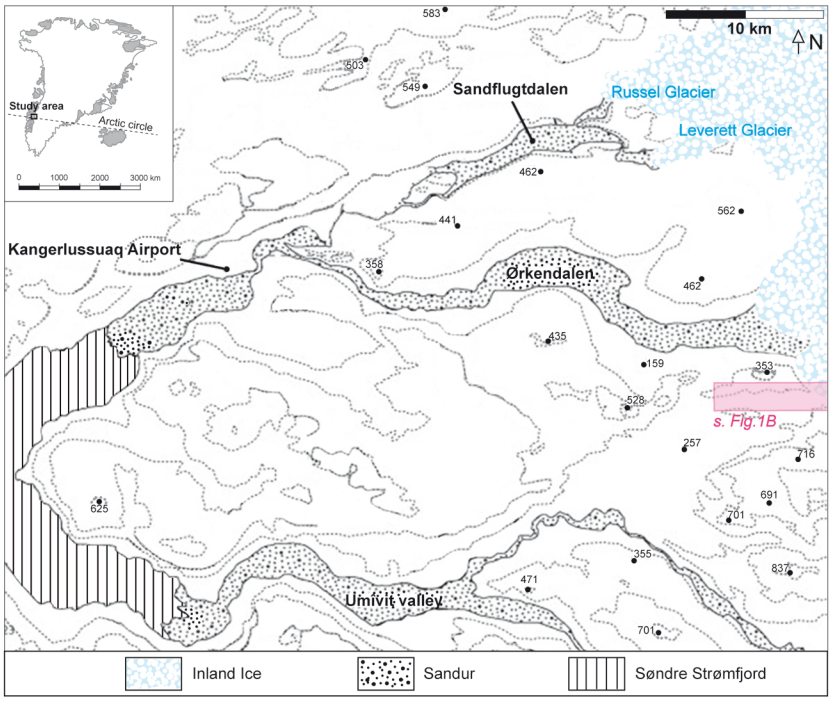
Study area
Arctic circle
0 1000 2000 3000 km
10 km
N
583
503
549
Sandflugtdalen
Russel Glacier
Leverett Glacier
462
441
562
Kangerlussuaq Airport
358
Ørkendalen
462
435
159
353
528
s. Fig.1B
257
716
691
625
701
355
837
471
Umivit valley
701
Inland Ice
Sandur
Søndre Strømfjord

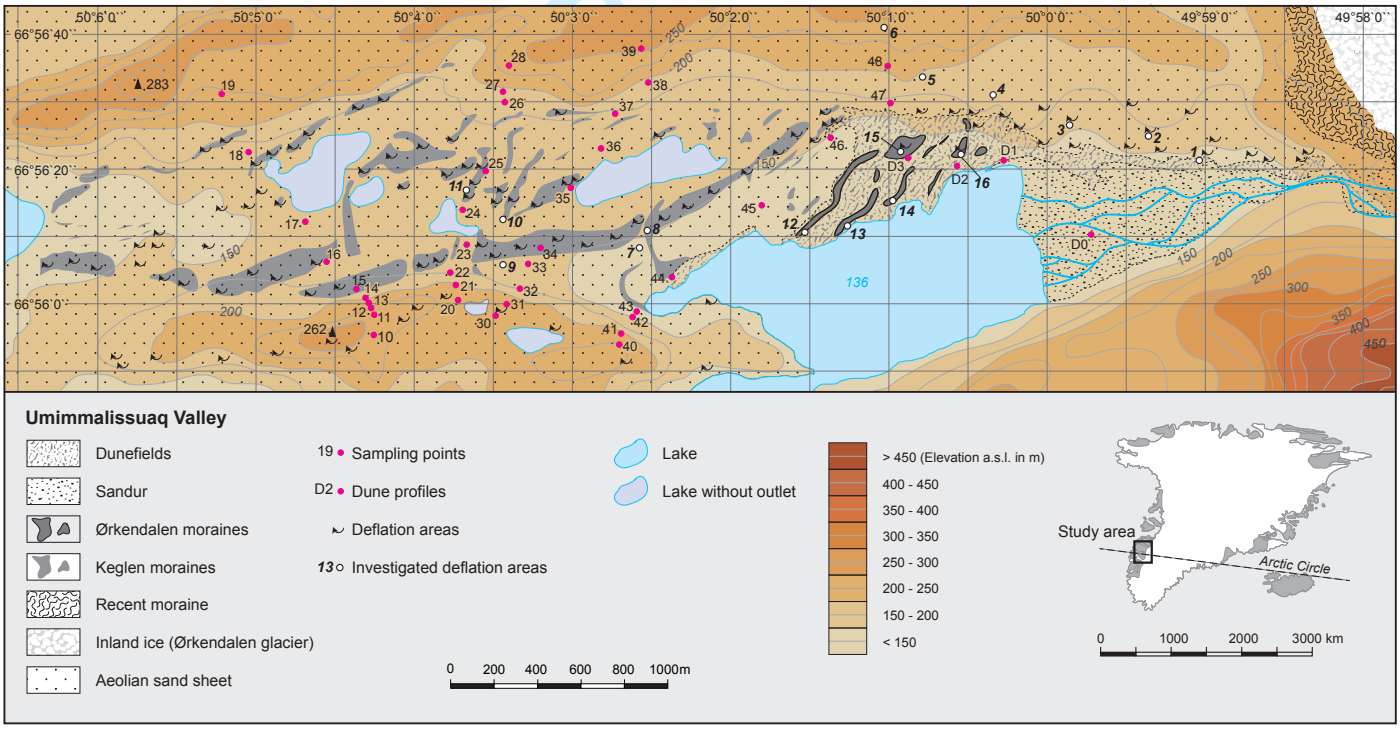
Umimmalissuaq Valley
Dunefields
Sandur
Ørkendalen moraines
Keglen moraines
Recent moraine
Inland ice (Ørkendalen glacier)
Aeolian sand sheet
19 Sampling points
D2 Dune profiles
Deflation areas
13 Investigated deflation areas
Lake
Lake without outlet
> 450 (Elevation a.s.l. in m)
400 - 450
350 - 400
300 - 350
250 - 300
200 - 250
150 - 200
< 150
0 200 400 600 800 1000m
Study area
Arctic Circle
0 1000 2000 3000 km

Figure 2. (a) Recent moraine of Ørkendalen glacier overrunning current vegetation. Photo (2014) was taken towards northwest.
812x609mm (72 x 72 DPI)

Figure 2. (b) Umimmalissuaq valley with the glacial outwash plain and the large dunefield west/northwest of the outwash plain (for locations see Figure 1b) - taken towards west/northwest.
1219x812mm (72 x 72 DPI)

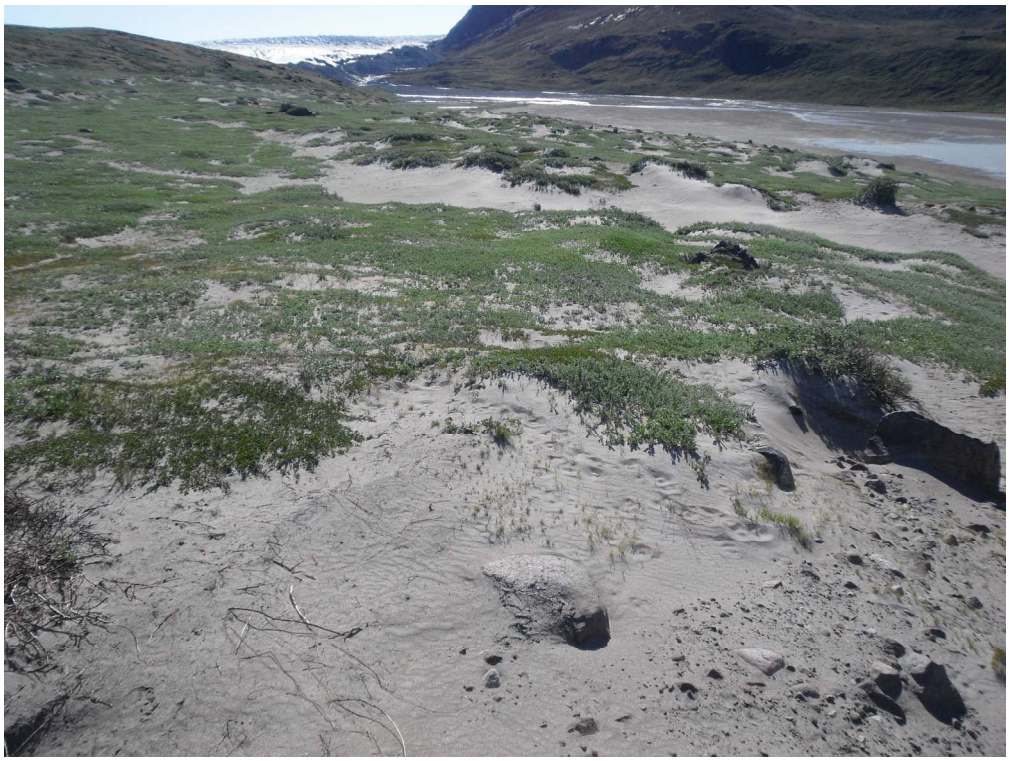

Figure 2. (c) Large dunefield, glacial outwash plain and Ørkendalen glacier - taken from profile D3 towards east.
812x609mm (72 x 72 DPI)

Figure 2. (d) Large dunefield, glacial outwash plain and Ørkendalen glacier - taken from profile D2 towards east.
1219x812mm (72 x 72 DPI)

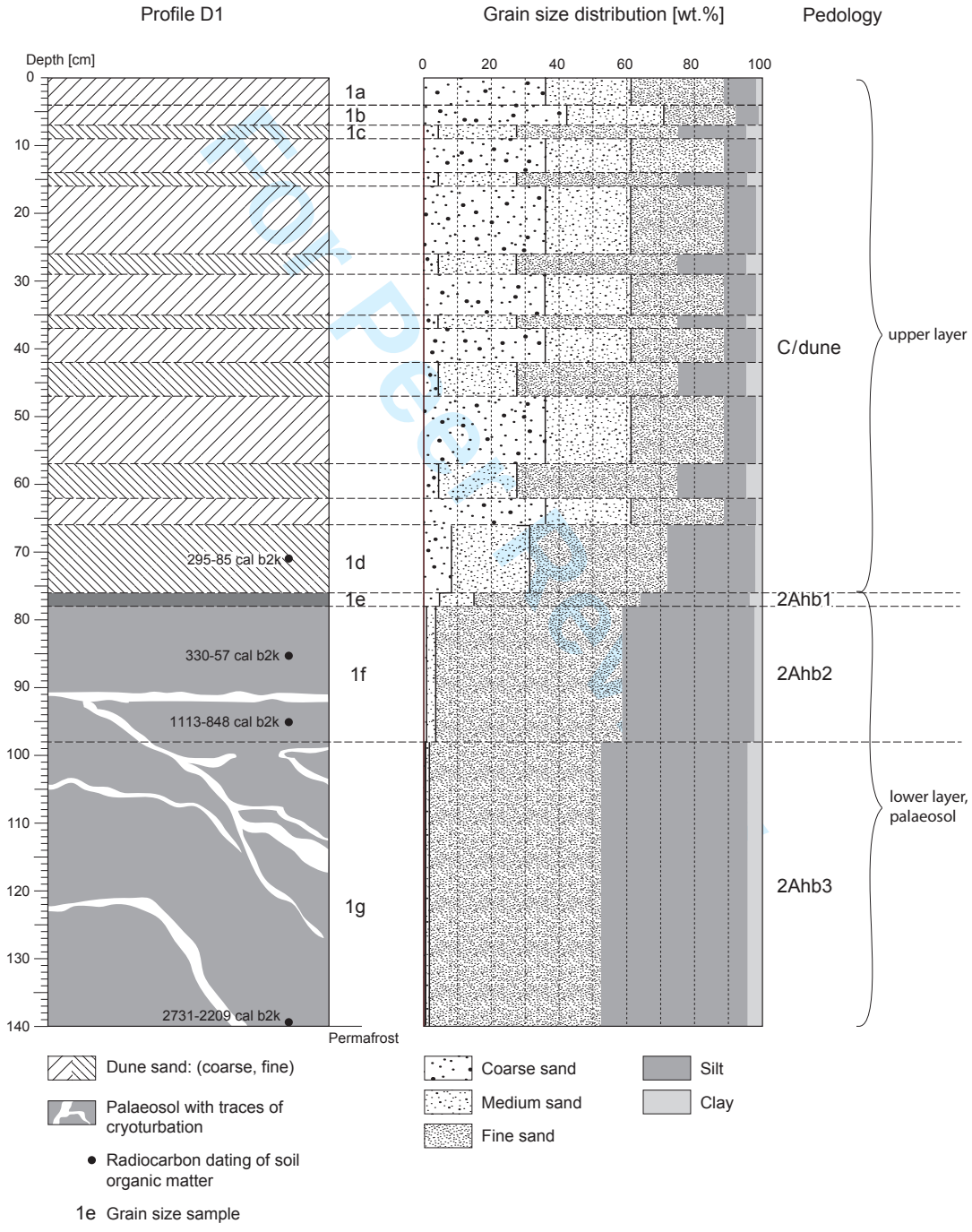
Profile D1
Grain size distribution [wt.%]
Pedology
Depth [cm]
0
10
20
30
40
50
60
70
80
90
100
110
120
130
140
0
20
40
60
80
100
1a
1b
1c
1d
1e
1f
1g
295-85 cal b2k
330-57 cal b2k
1113-848 cal b2k
2731-2209 cal b2k
Permafrost
C/dune
2Ahb1
2Ahb2
2Ahb3
upper layer
lower layer, palaeosol
Dune sand: (coarse, fine)
Palaeosol with traces of cryoturbation
Radiocarbon dating of soil organic matter
1e Grain size sample
Coarse sand
Medium sand
Fine sand
Silt
Clay

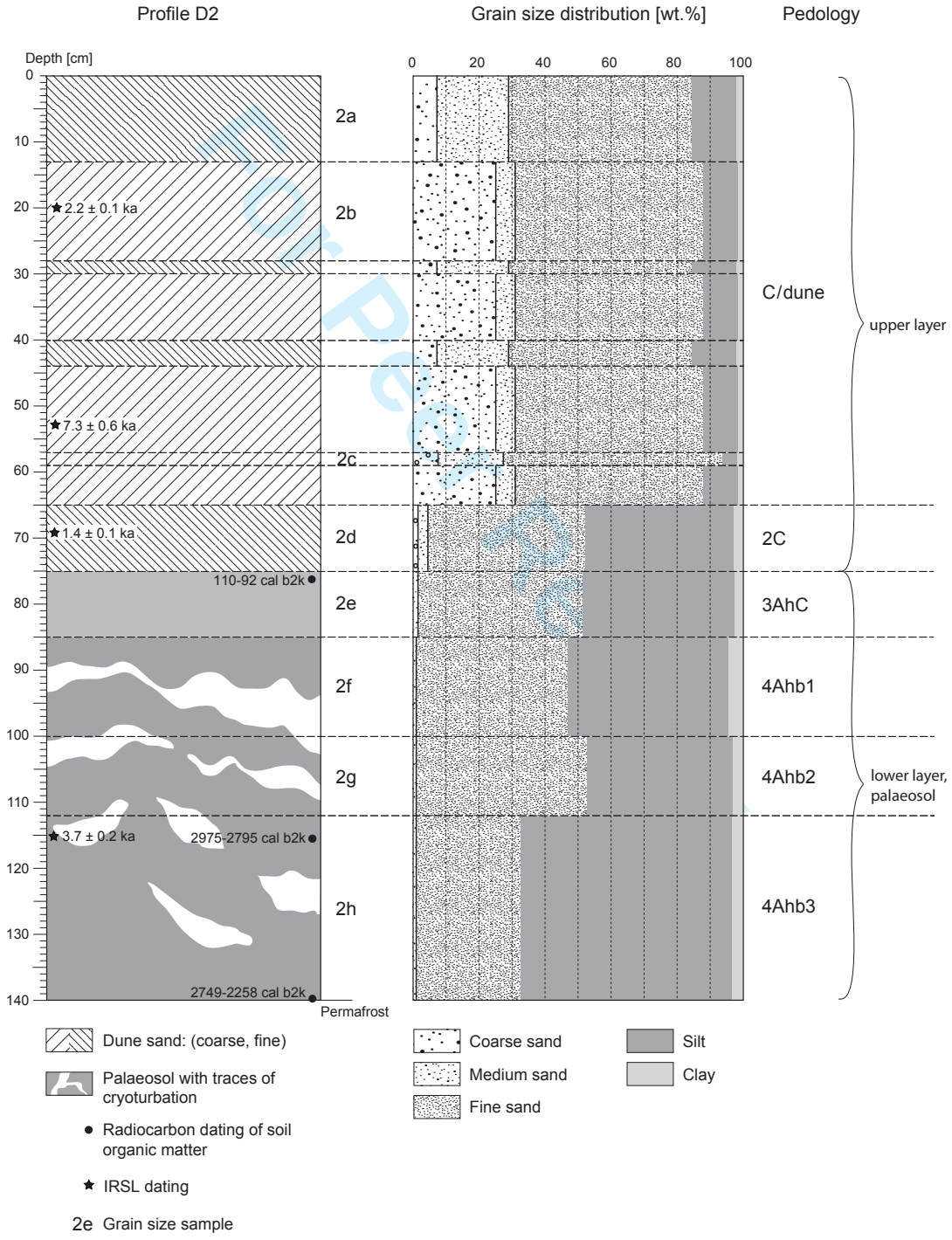
Profile D2
Grain size distribution [wt.%]
Pedology
Depth [cm]
0
10
20
30
40
50
60
70
80
90
100
110
120
130
140
0
20
40
60
80
100
2a
2b
2c
2d
2e
2f
2g
2h
2.2 ± 0.1 ka
7.3 ± 0.6 ka
1.4 ± 0.1 ka
110-92 cal b2k
3.7 ± 0.2 ka
2975-2795 cal b2k
2749-2258 cal b2k
Permafrost
C/dune
2C
3AhC
4Ahb1
4Ahb2
4Ahb3
upper layer
lower layer, palaeosol
Dune sand: (coarse, fine)
Palaeosol with traces of cryoturbation
Radiocarbon dating of soil organic matter
IRSL dating
2e Grain size sample
Coarse sand
Medium sand
Fine sand
Silt
Clay

Figure 3. (c) Photo of profile D1 showing palaeosol (lower layer) and overlying dune sand (upper layer). Traces of cryoturbation are present in palaeosol.
647x914mm (96 x 96 DPI)

Figure 3. (d) Photo of profile D2 showing palaeosol (lower layer) and overlying dune sand (upper layer). Traces of cryoturbation are present in palaeosol.
609x812mm (72 x 72 DPI)

Sedimentary unit	Location	Sand (± SD)	Silt (± SD)	Clay (± SD)
Upper + lower layer	Dunes	63 ± 20	35 ± 19	2 ± 1
	Cross-section 4	48 ± 16	49 ± 15	3 ± 2
	Cross-section 3	49 ± 17	47 ± 16	4 ± 3
	Cross-section 2	47 ± 16	50 ± 16	3 ± 2
	Cross-section 1	46 ± 14	50 ± 14	4 ± 2
Upper layer	Dunes	85 ± 8	13 ± 7	2 ± 1
	Cross-section 4	47 ± 12	49 ± 11	4 ± 2
	Cross-section 3	44 ± 7	51 ± 7	5 ± 5
	Cross-section 2	40 ± 7	57 ± 7	3 ± 2
	Cross-section 1	42 ± 6	54 ± 6	4 ± 2
Lower layer	Dunes	48 ± 9	49 ± 9	3 ± 1
	Cross-section 4	48 ± 21	50 ± 21	2 ± 2
	Cross-section 3	55 ± 23	42 ± 22	3 ± 2
	Cross-section 2	58 ± 21	39 ± 19	3 ± 3
	Cross-section 1	50 ± 20	46 ± 18	4 ± 2

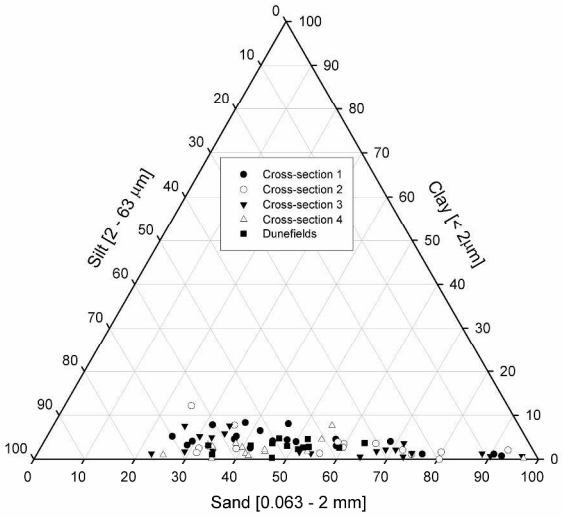

Figure 4. (a) Soil texture ternary diagrams (data shown in wt.%). Lower layer of cross-sections 1 to 4 compared to lower layer of dunefields. Dune profiles show relatively fine, the sampling points from cross-section 1 to 4 partly coarse grain sizes.
296x420mm (300 x 300 DPI)

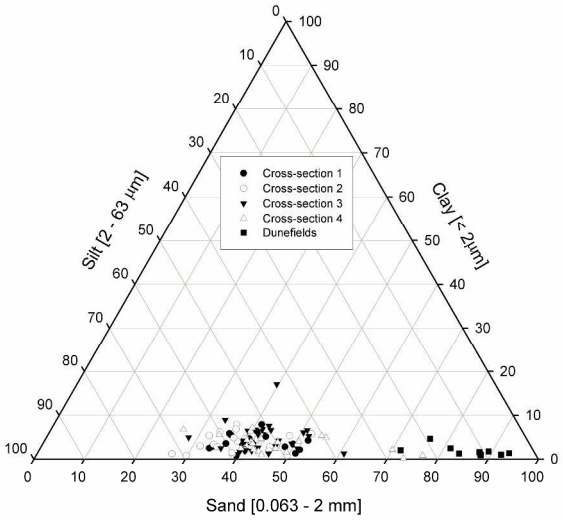

Figure 4. (b) Soil texture ternary diagrams (data shown in wt.%). Upper layer of cross-sections 1 to 4 compared to the upper layer of dunefields. Highest sand contents, particularly in both coarse and medium sand range, were found in the dunefields. Cross-section 4 has higher contents of sandy loam compared to cross-sections 1 to 3.
296x420mm (300 x 300 DPI)

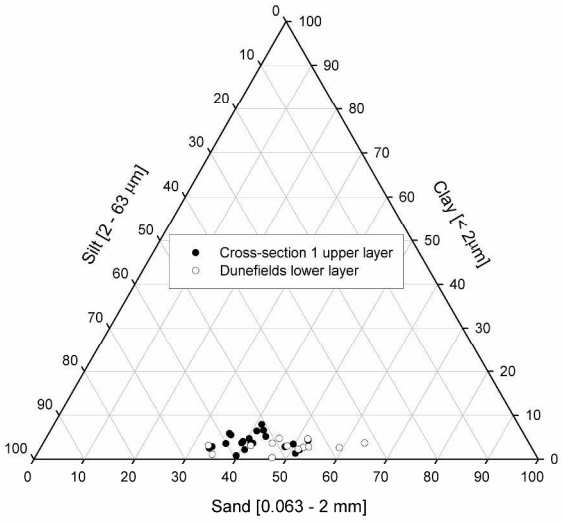

Figure 4. (c) Soil texture ternary diagrams (data shown in wt.%). Lower layer of dunefields compared to the upper layer of cross-section 1. Note that grain sizes from the lower layer of dune profiles are in the same range as from the upper layer of cross-section 1.
296x420mm (300 x 300 DPI)

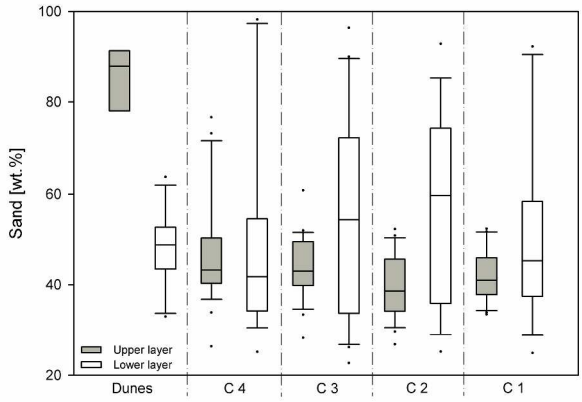

Figure 4. (d) Variability of sand content (wt.%) in the upper layer and lower layer of dune sediments (Dunes) and cross-sections 1 to 4 (C1, C2, C3, C4).
296x420mm (300 x 300 DPI)

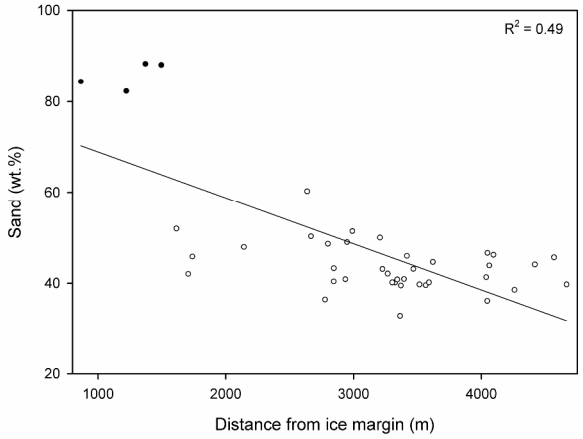

Figure 4. (e) Mean sand content (wt.%) in the upper layer of dune sediments (filled dots) and cross-sections 1 to 4 (blank dots) with increasing distance (m) from the ice margin.
296x420mm (300 x 300 DPI)

Chronological process	Lab-No.	Sampling point/Location	Calibrated age [cal b2k][a]	^{14}C age [BP]	Luminescence age [ka]	^{10}Be age [ka]	Material	Depth [cm]	Relevance [min./max. age]	Reference
Ørkendalen moraine formation	UtC-1987	Sandflugtdalen (67.09°N/50.29°W)	7533-7074	6380±100			Gyttja (mud)	200	Max. Ørkendalen moraines	Van Tatenhove et al. (1996)
	UtC-1990	Sandflugtdalen (67.09°N/50.34°W)	7208-6850	6090±50			Gyttja (mud)	No info	Max. Ørkendalen moraines	Van Tatenhove et al. (1996)
	LL0901-LL0911	Sandflugtdalen (67.11°N/50.29°W; 67.16°N/50.12°W)				6.8±0.3	Boulders	No info	Max. Ørkendalen moraines	Levy et al. (2012)
	UIC-1558	Sandflugtdalen (no data)			3.2-2.7		Org. material	35	Min. Ørkendalen moraines	Forman et al. (2007)
	UIC-1556	Sandflugtdalen (no data)			3.0-2.9		Org. material	28	Min. Ørkendalen moraines	Forman et al. (2007)
	Erl-16623	D2/Umimmalissuaq valley (66.56°N/50.0°W)	2975-2795	2709±50			Org. material	112-117	Min. Ørkendalen moraines	This study
	Erl-19004	D2/Umimmalissuaq valley (66.56°N/50.0°W)	2749-2258	2361±50			Org. material	140	Min. Ørkendalen moraines	This study
	Erl-19003	D1/Umimmalissuaq valley (66.56°N/50.0°W)	2731-2209	2333±51			Org. material	140	Min. Ørkendalen moraines	This study
	No info	H1/Sandflugtdalen (no data)	1941-1236	1605±160			Org. material	23-25	Min. Ørkendalen moraines	Ozols (2003)
	No info	G1/Sandflugtdalen (no data)	1866-1232	1550±145			Org. material	23-25	Min. Ørkendalen moraines	Ozols (2003)
	No info	Umimmalissuaq valley (no data)			1.4-1.0		Peaty silt	40	Min. Ørkendalen moraines	Scholz and Grottenthaler (1988)
	UW-180	Lake Ørkendalen (no data)	570-(-52)	330±75			Plant residues	No info	Min. Ørkendalen moraines	Ten Brink (1975)
Retreat of ice margin and start of soil formation (palaeosols)	UtC-2034	Sandflugtdalen (67.10°N/50.24°W)	4680-4490	4060±60			Peat	No info	Start of soil formation	Van Tatenhove et al. (1996)

	UtC-5624	PS4-Russell/P1 Base Sandflugtdalen (67.05°N/50.14°W)	3869-3123	3200±130	Plant residues	No info	Halt in aeolian sand formation	Willemse et al. (2003)
	GrN-14655	Sand sheet Sandflugtdalen (67.03°N, 50.24°W)	3442-3263	3095±40	Sandy peat	No info	Halt in aeolian sand formation	Dijkmans and Törnqvist (1991)
	Erl-16623	D2/Umimmalissuaq valley (66.56°N/50.0°W)	2975-2795	2709±50	Org. material	112-117	Min. Ørkendalen moraines, start of soil formation	This study
	Erl-19004	D2/Umimmalissuaq valley (66.56°N/50.0°W)	2749-2258	2361±50	Org. material	140	Min. Ørkendalen moraines	This study
	Erl-19003	D1/Umimmalissuaq valley (66.56°N/50.0°W)	2731-2209	2333±51	Org. material	140	Min. Ørkendalen moraines	This study
Readvance of ice margin and (re)accumulation of aeolian sand	Erl-16621	D1/Umimmalissuaq valley (66.56°N/50.0°W)	1113-848	1041±50	Org. material	93-98	Halt in soil formation and (re)accumulation of aeolian sand	This study
	Erl-19002	D1/Umimmalissuaq valley (66.56°N/50.0°W)	330-57	123±47	Org. material	85	Halt in soil formation and (re)accumulation of aeolian sand	This study
	Erl-16620	D1/Umimmalissuaq valley (66.56°N/50.0°W)	295-85	-204±45	Org. material	66-76	Halt in soil formation and (re)accumulation of aeolian sand	This study
	Erl-16622	D2/Umimmalissuaq valley (66.56°N/50.0°W)	110-92	-349±44	Org. material	71-76	Halt in soil formation and (re)accumulation of aeolian sand	This study
	GrN-14651	Sand sheet Ørkendalen (67.0°N/50.28°W)	735-560	610±80	Peaty silt	No info	(Re)accumulation of aeolian sand	Dijkmans and Törnqvist (1991)
	UtC-5619	PS4-Russell/P1 Top Sandlugtdalen (67.05°N/50.14°W)	595-550	487±30	Plant residues	No info	(Re)accumulation of aeolian sand	Willemse et al. (2003)

Additional data	Erl-19000	17/ Umimmalissuaq valley (66.56°N/50.47°W)	5335-4919	4433±54	Org. material	50	Min. Umîvît/Keglen, max. Ørkendalen moraines	This study
	Erl-16614	33/Umimmalissuaq valley (66.56°N/50.33°W)	4876-4499	4114±53	Org. material	60-62	Min. Umîvît/Keglen, max. Ørkendalen moraines	This study
	Erl-19001	24/ Umimmalissuaq valley (66.56°N/50.37°W)	2975-2800	2720±49	Org. material	80	Min. Umîvît/Keglen, max. Ørkendalen moraines	This study
	Erl-16619	D0/Umimmalissuaq valley (66.56°N/49.59°W)	310-76	7±45	Org. material	44-47		This study

[a] Calibration was conducted using Oxcal version 4.2 (Bronk Ramsey, 2009)

Field ID	Laboratory ID	Sampling depth (cm)	^{226}Ra ± s.e. (Bq/kg)	^{232}Th ± s.e. (Bq/kg)	^{40}K ± s.e. (Bq/kg)	Water content (%)	Total dose rate ± s.e. (Gy/ka)	n	De ± s.e. (Gy)	*g*-value (%/decade)	age ± s.e. (ka)	Fading corrected age ± s.e. (ka)
D2 - 20	143078	20	2.83 ± 0.27	7.48 ± 0.33	486 ± 10	10.6	2.37 ± 0.08	12	3.2 ± 0.2	3.81 ± 0.17	1.6 ± 0.1	2.2 ± 0.1
D2 - 53	143079	53	3.49 ± 0.25	7.73 ± 0.26	453 ± 8	7.5	2.33 ± 0.08	12	12.8 ± 0.8	3.13 ± 0.20	5.5 ± 0.4	7.3 ± 0.6
D2 - 69	143080	69	6.62 ± 0.31	11.30 ± 0.39	453 ± 9	23.9	2.17 ± 0.07	12	2.4 ± 0.1	2.87 ± 0.03	1.1± 0.1	1.4 ± 0.1
D2 - 115	143081	115	7.62 ± 0.47	11.60 ± 0.56	404 ± 11	22.9	2.04 ± 0.07	12	5.7 ± 0.1	3.33 ± 0.12	2.8 ± 0.1	3.7 ± 0.2

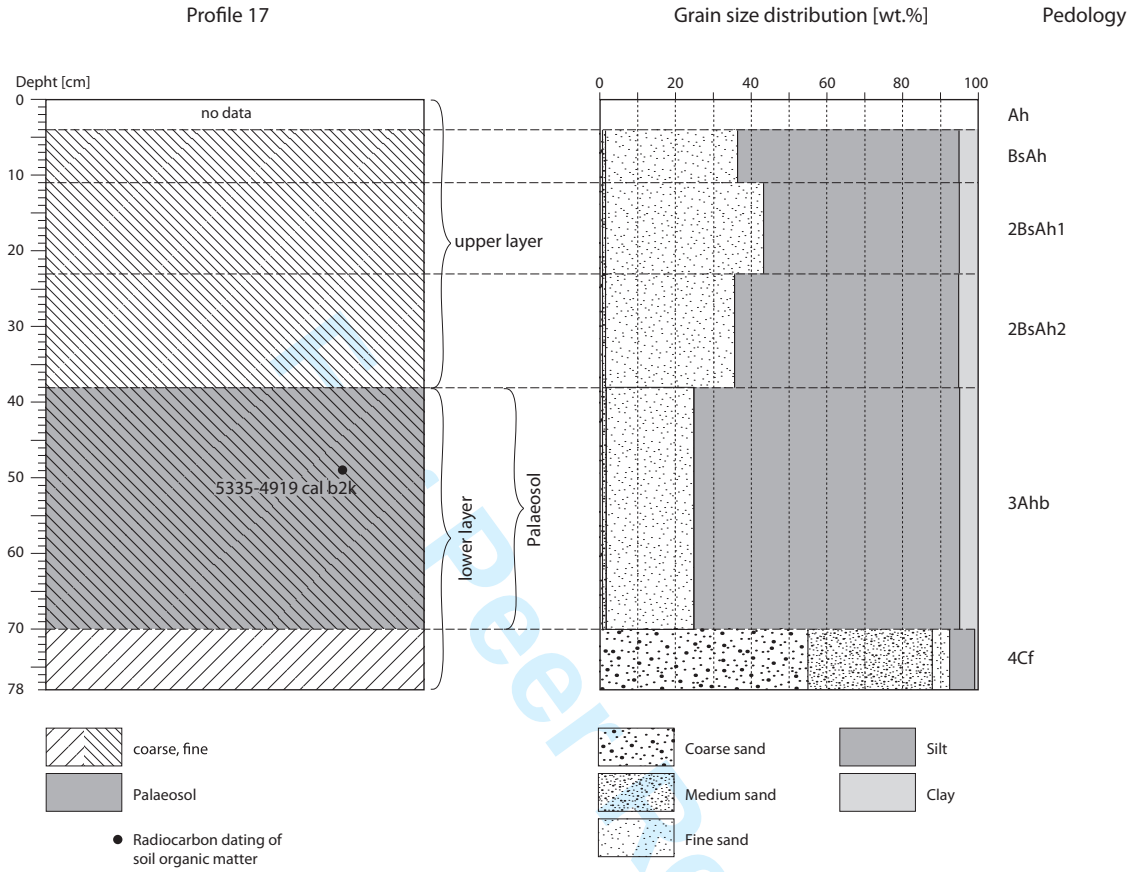

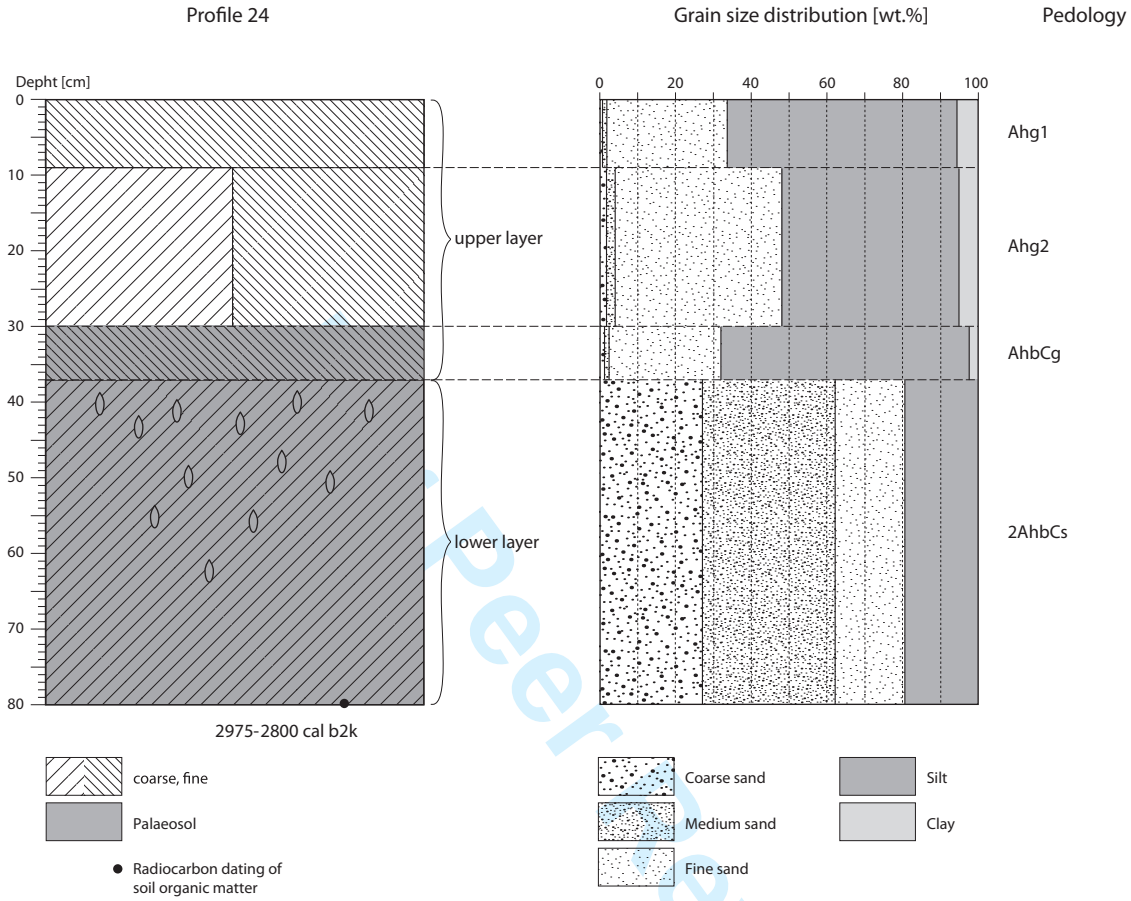

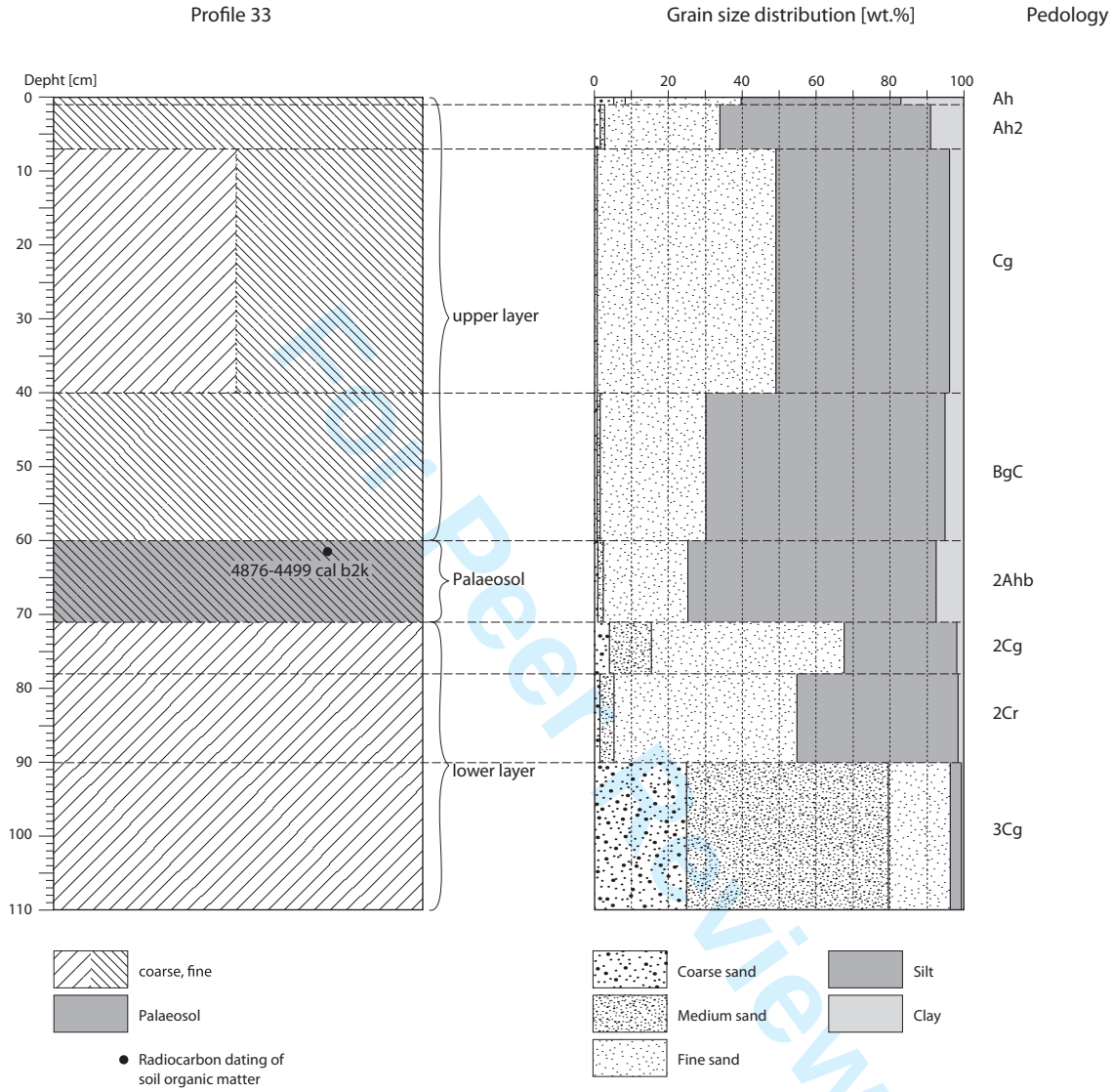

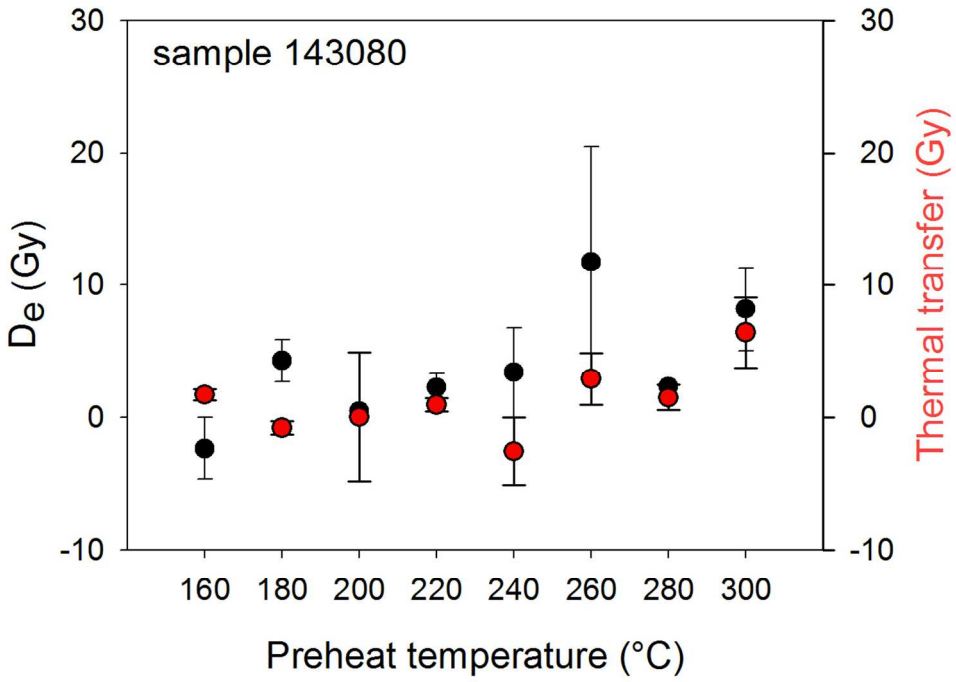

114x82mm (300 x 300 DPI)

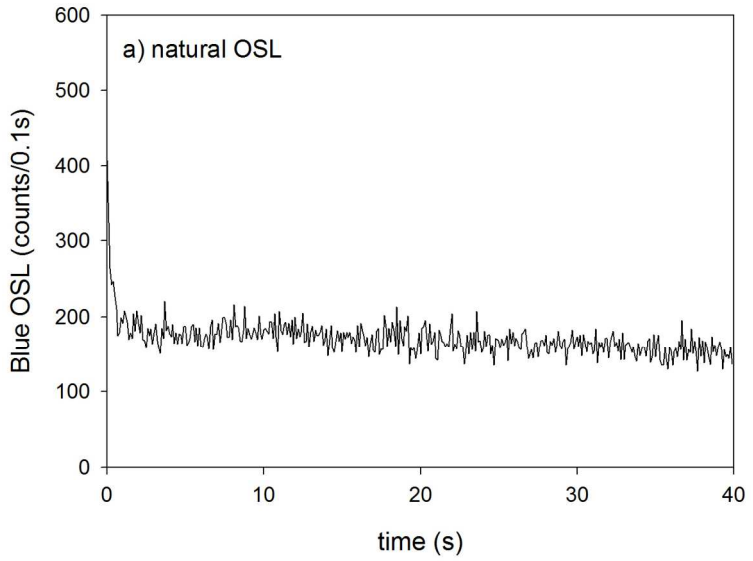

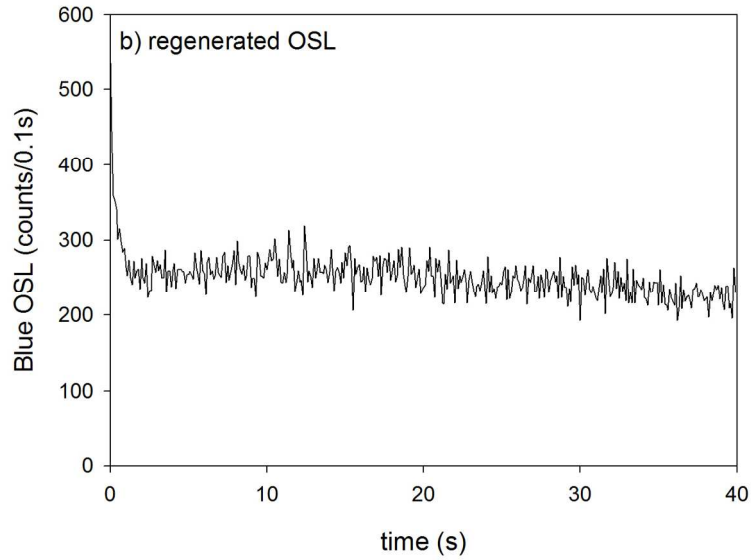

121x181mm (300 x 300 DPI)

Profile	Horizon	Depth [cm]	cS	mS	fS	ffS	Sand Sum	cU	mU	fU	Silt Sum	Clay Sum
10-1	OiOe	-3	1.3	1.3	2.2	29.1	34	55.8	6.5	0.9	63	2.8
10-2	Ah	-9	0.3	1.0	2.0	30.3	34	54.6	8.0	1.4	64	2.5
10-3	2Ah	-12	0.5	1.1	2.2	32.4	36	52.7	6.3	1.2	60	3.6
10-4	2C/Ahb	-38	0.4	0.9	2.9	36.5	41	47.4	8.6	1.1	57	2.2
10-5	2Bhs	38-55+	1.7	2.5	2.2	22.4	29	53.3	13.7	1.0	68	3.2
11-1	CfAh1	-50	0.2	1.2	6.1	50.1	58	34.6	2.7	0.6	38	4.5
11-2	CfAh2	-75					No data					
11-3	CfAh3	-100					No data					
11-4	CfAh4	-125					No data					
12-1	Ah	-3	0.9	1.3	3.6	34.6	40	45.9	8.3	0.8	55	4.7
12-2	CAh	-22	0.8	2.0	4.3	35.2	42	42.6	6.7	1.8	51	6.6
12-3	Cfh	22+	0.6	1.4	6.2	44.3	53	38.0	4.4	0.5	43	4.5
13-1	Ah	-6	1.3	2.1	3.4	34.2	41	43.2	8.0	1.4	53	6.4
13-2	CAh1	-27	0.2	0.6	5.0	46.5	52	38.2	5.0	0.3	43	4.3
13-3	CAh2	-49	0.7	1.1	3.1	36.7	42	44.8	7.0	0.0	52	6.5
13-4	C	-60	2.7	4.4	3.4	27.0	37	46.9	10.7	0.3	58	4.6
13-5	Ah	-80	1.4	2.8	2.9	24.4	32	45.7	12.4	2.5	61	7.8
13-6	C	-90	12.3	13.1	5.2	17.4	48	36.2	10.6	0.7	48	4.4
13-7	Ah	-95	6.8	9.6	4.5	16.6	38	40.8	13.7	2.7	57	5.2
13-8	C	95-117+	10.1	16.6	6.9	16.4	50	33.7	10.8	1.5	46	4.0
14-1	Ah	-2	0.4	0.8	2.5	35.6	39	49.5	6.1	1.3	57	3.7
14-2	AhC	-27	0.0	1.1	4.7	42.4	48	41.9	6.3	0.5	49	2.8
14-3	2CAhb	-31	12.8	17.0	8.0	20.6	58	29.0	7.8	1.7	39	3.1
14-4	2C	31-45+	10.0	25.6	14.4	18.7	69	17.2	7.6	2.5	27	4.0
15-1	CAh	-18	1.1	0.6	5.3	44.3	51	39.5	7.5	0.5	47	1.3
15-2	AhbC	-40	0.1	0.3	3.5	37.3	41	45.2	4.3	1.3	51	7.9
15-3	2Ahb	-45	0.2	0.4	4.1	41.8	46	37.6	6.4	1.5	46	8.1
15-4	2AhbC	-65	0.0	0.4	2.3	35.1	38	49.7	3.5	0.7	54	8.3
15-5	3Ahb	-67					No data					

15-6	3Bgb	-74	1.2	2.7	2.5	23.0	29	50.0	14.9	1.6	67	4.1
16-1	Ah	-12	0.3	1.1	2.8	35.2	39	48.0	7.2	1.3	57	4.0
16-2	CAh	-22	0.1	0.7	3.0	37.4	41	46.3	7.7	1.0	55	3.7
16-3	2CAhb	-38	0.0	0.3	4.7	46.5	52	38.6	6.5	1.2	46	2.2
16-4	3C	38+	0.1	0.2	2.8	38.5	42	46.8	7.9	1.1	56	2.6
17-1	Ah	-4					No data					
17-2	BsAh	-11	0.2	0.3	2.7	33.1	36	49.4	7.8	1.0	58	5.5
17-3	2BsAh1	-23	0.1	0.4	3.7	39.2	43	43.6	7.1	0.7	51	5.2
17-4	2BsAh2	-38	0.2	0.2	2.0	33.4	36	48.4	8.7	1.2	58	5.9
17-5	3Ahb	-70	0.1	0.6	2.0	22.2	25	50.5	16.0	3.5	70	5.2
17-6	4Cf	-78+ PF	55.0	33.7	1.8	1.8	92	3.3	1.7	1.9	7	0.7
18-1	CAh	-7					No data					
18-2	Ahb	-22	0.1	0.5	3.6	37.4	42	45.1	7.7	2.0	55	3.6
18-3	2CAhb	-28	0.1	0.5	4.7	44.4	50	39.6	5.8	1.4	47	3.5
18-4	3Ahb	28-40+	0.2	0.4	4.2	40.4	45	42.7	6.8	1.0	51	4.2
19-1	Ah	-2	7.4	10.0	4.8	17.5	40	42.0	14.9	2.6	59	0.8
19-2	AC	-36	24.8	26.6	9.6	15.5	76	17.2	4.4	0.8	22	1.2
19-3	2C	36-40+	19.9	49.9	12.0	8.8	91	4.6	3.1	0.5	8	1.2
20-1	Ah	-6	0.5	2.0	4.0	38.9	45	46.0	5.0	0.8	52	2.8
20-2	AhC	-21	0.4	1.0	5.6	42.8	50	41.1	6.8	1.5	49	0.8
20-3	CAh	-36	0.8	2.6	3.4	32.0	39	49.1	9.7	1.2	60	1.2
20-4	C	-42	1.6	4.9	5.1	27.4	39	46.3	10.9	1.4	59	2.4
21-1	Oi	-6					No data					
21-2	AhC	-32	0.2	0.9	3.9	34.7	40	44.2	8.9	2.5	56	4.8
21-3	Ahb	-40	0.4	3.1	3.3	29.1	36	45.4	9.2	1.8	56	7.8
22-1	Ah	-3	0.3	0.6	2.2	33.2	36	46.3	6.9	2.6	56	7.9
22-2	CrAh	-22	1.0	1.2	6.7	43.4	52	35.5	5.1	1.5	42	5.8
22-3	AhCr	-47	0.1	0.3	1.9	29.8	32	50.8	8.9	2.8	63	5.4
22-4	2Oe	-61	0.3	1.0	1.9	22.0	25	47.7	10.7	4.3	63	12.2
22-5	2Oi	-70					No data					
22-6	3C	-82+	5.9	28.6	21.3	24.2	80	14.7	2.7	1.1	18	1.6

23-1	Ah	-2	0.3	2.5	3.1	30.8	37	47.3	7.4	1.8	56	6.9
23-2	AhgC	-28	0.1	0.5	3.5	38.7	43	45.0	7.2	0.8	53	4.2
23-3	Bs	-33	9.9	21.5	11.0	17.4	60	24.2	10.3	2.3	37	3.5
23-4	2Cg	-41	13.7	25.2	11.9	15.1	66	18.6	9.9	1.9	30	3.6
23-5	3C	-44	12.0	16.1	11.8	20.0	60	24.8	10.6	2.0	37	2.7
23-6	4C	-59	1.4	10.7	14.5	31.7	58	30.6	6.8	0.4	38	3.9
23-7	5Cd	-78+	22.4	48.9	13.0	8.7	93	3.8	1.0	0.1	5	2.1
24-1	Ahg1	-9	0.3	0.7	2.7	30.1	34	50.8	7.6	1.7	60	6.2
24-2	Ahg2	-30	1.5	2.3	4.4	39.8	48	38.3	5.5	2.8	47	5.4
24-3	AhbCg	-37	1.1	1.2	1.8	27.4	31	53.5	11.3	1.3	66	2.5
24-4	2AhbCs	-70+	26.8	35.5	8.4	9.7	80	12.9	5.2	1.5	20	0.0
25-1	Ah	-4	0.2	0.3	1.8	31.6	34	55.0	6.5	1.3	63	3.4
25-2	CAh	-10	0.0	0.3	3.3	37.3	41	46.3	9.2	1.7	57	2.0
25-3	2C1	-21	0.6	0.6	1.7	26.8	30	57.3	10.1	1.9	69	0.9
25-4	2C2	-34	3.3	3.7	2.2	17.6	27	54.3	15.9	1.7	72	1.2
25-5	3C	-49+	24.9	28.0	10.5	10.9	74	16.4	6.9	1.3	25	1.1
26-1	Ah	-23	0.0	0.4	3.6	37.9	42	43.7	7.1	2.6	53	4.6
26-2	AhC	-40	0.0	0.2	2.2	35.9	38	49.7	6.7	1.2	58	4.1
26-3	C	-50	0.1	0.4	2.0	29.0	32	53.3	12.2	1.5	67	1.5
26-4	2C	-100+	17.5	21.9	5.5	11.2	56	30.5	11.2	1.0	43	1.3
27-1	AhC1	-3	1.6	3.1	5.2	36.6	47	41.9	7.3	1.1	50	3.2
27-2	AhC2	-8	0.1	1.0	4.0	32.1	37	46.5	10.2	1.1	58	4.9
27-3	2Ahb	-12	0.1	0.6	4.5	45.5	51	39.3	6.3	0.4	46	3.2
27-4	3AhC1	-27	0.0	0.3	2.4	32.2	35	52.6	8.8	0.9	62	2.8
27-5	3AhC2	-40	0.9	3.6	3.3	23.6	31	50.4	13.8	1.3	65	3.0
28-1	Ah	-1	12.6	5.9	3.3	23.9	46	39.5	11.8	1.2	52	1.9
28-2	C	-18	9.4	9.1	3.9	16.0	39	42.6	15.5	1.9	60	1.5
28-3	2C	-78+	13.4	27.5	13.9	17.3	72	14.7	8.0	3.0	26	2.1
30-1	Ah	-7	0.7	1.7	4.2	39.7	46	42.3	6.1	1.0	49	4.3
30-2	CAh1	-15	0.0	0.4	3.7	36.6	41	46.5	9.0	1.7	57	2.0
30-3	CAh2	-41	0.1	0.4	3.0	38.7	42	46.7	8.3	0.8	56	1.9

30-4	2C	-63	30.3	33.5	12.8	11.6	88	6.6	3.3	0.6	11	1.3
30-5	3C	-83	15.2	30.1	13.0	16.0	74	15.0	7.4	1.9	24	1.4
31-1	Ah	-4	1.4	2.3	3.4	34.5	42	44.6	6.7	1.4	53	5.6
31-2	CAh	-13	0.5	2.0	5.5	37.9	46	41.5	10.0	1.3	53	1.3
31-3	2CAh1	-40	0.3	0.5	5.7	43.9	50	37.2	5.9	0.3	44	6.1
31-4	2CAh2	-75	0.9	1.0	2.0	31.1	35	48.9	8.0	0.5	57	7.6
32-1	Ah	-4					No data					
32-2	C1	-12	0.0	0.3	4.5	38.3	43	47.8	5.7	0.7	54	2.7
32-3	C2	-39	0.9	1.3	2.3	31.3	36	50.3	10.2	1.1	62	2.5
32-4	2C	-115	9.0	27.0	15.5	20.1	72	16.5	5.9	2.4	25	3.7
33-1	Ah	-1	5.9	2.1	2.8	28.8	40	30.7	9.6	3.0	43	17.0
33-2	Ah2	-7	1.7	1.3	2.1	28.4	33	49.3	6.5	1.8	58	8.9
33-3	Cg	-40	0.0	0.3	4.4	44.5	49	40.3	5.4	1.3	47	3.6
33-4	BgC	-60	0.3	0.7	2.4	26.8	30	51.6	10.5	2.4	65	5.2
33-5	2Ahb	-71	0.5	1.3	2.3	22.0	26	47.8	14.3	4.2	66	7.6
33-6	2Cg	-78	3.9	11.9	16.8	34.4	67	24.0	5.4	1.8	31	1.8
33-7	2Cr	-90	1.2	4.1	9.3	39.6	54	34.4	8.2	1.8	44	1.4
33-8	3Cg	-110	24.2	54.9	11.3	6.1	96	2.4	0.4	0.1	3	0.7
34-1	Ah	-4	0.2	0.9	2.2	36.5	40	47.5	6.8	1.7	56	4.2
34-2	CAh	-26	0.2	1.2	4.2	40.8	46	43.6	6.2	0.7	51	3.0
34-3	C	-45+	1.3	1.8	2.2	23.7	29	53.5	13.8	1.9	69	1.8
35-1	Ah	-5	0.6	2.0	4.1	32.4	39	42.0	9.3	3.0	54	6.5
35-2	Bg	-43	0.7	4.2	10.4	45.6	61	33.5	3.8	0.6	38	1.3
35-3	Wrl1	-52	0.7	4.1	12.2	34.8	52	38.4	6.9	1.3	47	1.6
35-4	Wrl2	-52+	0.1	12.5	39.6	37.8	90	8.4	0.4	0.3	9	0.7
36-1	Ah	-9	2.7	11.2	7.7	29.3	51	35.3	5.4	1.8	42	6.6
36-2	CAh	-48	2.0	4.0	8.1	37.7	52	38.1	3.6	1.1	43	5.3
36-3	2CAh	-94	0.3	1.3	4.1	42.4	48	42.1	5.7	0.0	48	4.1
37-1	Ah	-8	0.3	1.5	3.9	37.2	43	40.1	7.8	1.7	50	7.6
37-2	CAh1	-47	0.1	0.5	3.5	39.6	44	41.6	6.5	1.5	50	6.7
37-3	CAh2	-61	0.0	0.3	2.1	32.5	35	50.3	5.4	3.5	59	5.9

37-4	2CAhb		0.0	0.2	1.5	31.1	33	52.2	7.9	2.2	62	5.0
38-1	Ah	-5	0.0	0.2	1.2	26.8	28	56.9	8.4	1.5	67	5.0
38-2	CAh1	-16	0.1	0.2	3.5	37.2	41	46.6	9.0	1.4	57	2.0
38-3	CAh2	-30	0.0	0.1	2.3	37.5	40	48.4	9.1	0.8	58	1.7
38-4	2C	-46	0.2	0.6	1.6	20.2	23	58.7	15.4	2.0	76	1.3
38-5	3C1	-71	9.1	25.3	12.8	17.1	64	19.7	11.5	3.9	35	0.6
38-6	3C2	-71+	15.3	26.5	14.0	17.1	73	15.5	7.8	3.1	26	0.6
39-1	Ah	-6	3.7	4.8	4.5	36.5	49	39.7	6.1	1.3	47	3.5
39-2	CAh	-35	0.9	1.6	4.6	44.0	51	39.9	6.1	0.5	46	2.4
39-3	2Ahb	-58	0.9	1.3	2.1	30.4	35	52.5	9.1	2.0	64	1.8
39-4	3C	-79	14.8	25.7	12.5	15.7	69	18.8	7.6	2.8	29	2.2
39-5	4C	-79+	15.3	26.7	12.6	16.0	71	15.0	8.7	3.5	27	2.2
40-1	AhC	-10	1.0	1.5	3.2	35.3	41	45.4	8.6	1.0	55	4.0
40-2	CAhg	-20	0.9	1.4	5.0	43.2	51	39.6	5.2	0.6	45	4.1
40-3	CAhgb	-37	0.7	1.2	5.2	48.3	55	32.4	4.7	2.5	40	5.0
40-4	Oeg	-43	0.5	1.1	5.6	48.1	55	31.7	3.3	2.0	37	7.6
40-5	Arhf	-50	0.5	1.8	5.2	47.2	55	36.2	3.6	0.9	41	4.5
41-1	OaAh	-14	2.9	2.5	3.4	30.9	40	49.4	4.0	0.5	54	6.5
41-2	Ah	-20	0.4	1.0	3.8	34.9	40	45.3	8.3	2.0	56	4.4
41-3	Oef	-20+	0.2	1.1	4.3	37.2	43	42.5	6.3	1.9	51	6.6
42-1	Ah	-4	0.4	1.5	3.1	34.7	40	43.0	7.9	2.2	53	7.2
42-2	AhC	-23	0.1	0.4	3.4	37.7	42	46.4	7.1	1.8	55	3.2
42-3	2Ch	-39	4.9	8.2	4.2	22.5	40	42.2	12.9	2.6	58	2.4
42-4	3CAhb	-50	1.5	2.3	2.6	31.8	38	46.1	10.4	1.7	58	3.6
42-5	4C	-52	5.3	7.2	4.3	23.2	40	42.5	12.7	2.1	57	2.7
42-6	5C	-54	8.0	11.7	5.4	19.9	45	39.4	11.2	2.7	53	1.7
43-1	Ah	-10	2.1	3.0	6.8	34.4	46	41.4	7.0	1.3	50	3.9
43-2	2Cg	-13	4.1	23.2	16.4	29.4	73	22.2	3.3	1.2	27	0.1
43-3	2AhgC	18-27	0.0	0.4	3.2	22.7	26	37.1	21.1	8.8	67	6.7
43-4	3Ahgb	54-77	1.7	5.1	4.9	21.2	33	48.1	13.2	2.6	64	3.3
44-1	CAh	-26	3.4	7.8	8.5	57.0	77	20.5	1.2	0.8	23	0.8

44-2	AhbC	-31	0.2	1.2	4.3	38.2	44	45.8	8.3	0.5	55	1.4
44-3	CAhb	-45	0.5	2.4	5.9	44.6	53	39.3	5.2	0.3	45	1.7
44-4	AhbC	-76	0.0	0.6	2.7	38.0	41	49.4	7.2	0.7	57	1.3
45-1	Ah	-6	1.1	12.5	10.3	30.5	54	34.2	4.9	1.2	40	5.3
45-2	CAh	-14	0.1	0.4	4.5	37.7	43	42.8	7.9	2.0	53	4.6
45-3	2AhbC	-45	0.0	0.4	4.3	42.0	47	42.7	5.9	2.3	51	2.5
45-4	2C	-70+	2.9	7.0	5.5	29.3	45	41.5	10.1	1.6	53	2.2
46-1	Ah	-12	0.5	4.8	3.9	34.3	44	44.6	8.3	1.7	55	1.8
46-2	C	-24	0.0	0.4	4.4	39.8	45	45.8	7.9	0.7	54	1.0
46-3	AhbC	-30	0.0	0.3	4.9	44.2	49	41.4	7.4	0.4	49	1.5
46-4	C	-52	1.7	5.8	3.0	31.7	42	47.1	10.0	0.0	57	0.8
46-5	2C	-95	28.0	64.1	5.3	0.9	98	0.2	1.3	0.9	2	0.1
46-6	3C	-100+	0.2	54.9	29.8	12.0	97	2.5	0.2	0.1	3	0.2
47-1	AhC	-10	0.3	14.7	16.1	38.9	70	26.5	1.6	0.3	28	2.1
47-2	Ahb	-20	0.1	0.7	2.4	30.7	34	49.5	9.1	1.8	60	5.6
47-3	CAhb	-70	0.1	0.7	2.3	30.5	34	53.8	8.5	1.4	64	2.8
47-4	C	-95+	0.1	0.2	2.4	31.3	34	52.9	9.0	1.3	63	2.9
48-1	AhC1	-15	0.0	0.4	3.5	37.7	42	44.9	8.8	1.1	55	3.6
48-2	AhC2	-30	0.0	0.3	3.7	38.4	42	46.1	8.3	1.0	55	2.2
48-3	C1	-45	2.5	0.1	1.5	31.2	35	53.9	9.2	1.5	65	0.1
48-4	C2	-65	0.5	1.0	2.1	21.6	25	57.0	14.6	2.2	74	1.0
D0-a	C/dune	-20	16.3	35.5	18.8	17.0	88	9.0	1.4	0.5	11	1.6
D0-b	C/dune	-44	4.1	23.3	20.8	33.3	81	15.1	1.0	0.1	16	2.5
D0-c	C/dune	-47	16.9	46.8	8.8	13.4	86	9.3	2.0	0.7	12	2.2
D0-d	2Ahb1	-57	17.2	20.8	6.0	27.1	71	22.4	2.9	1.0	26	2.7
D0-e	2Ahb2	58+	13.2	19.8	6.6	26.3	66	26.4	4.0	0.4	31	3.3
D1-a	C/dune	-4	36.1	25.5	10.6	17.2	89	7.7	1.3	0.1	9	1.8
D1-b	C/dune	-7	44.7	26.3	9.1	12.0	92	6.3	0.4	0.1	7	1.0
D1-c	C/dune	-10	4.6	22.8	12.9	35.9	76	18.7	0.1	0.3	19	4.7
D1-d	C/dune	55-65	8.8	22.4	11.1	29.4	72	25.3	0.7	0.2	26	2.1
D1-e	2Ahb1	65-67	4.8	9.7	6.8	42.5	64	29.2	3.1	0.4	33	3.7

D1-f	2Ahb2	-98	0.6	3.1	9.7	45.8	59	35.0	2.9	0.2	38	2.6
D1-g	2Ahb3	99+	0.2	0.9	4.9	46.0	52	37.9	4.4	1.0	43	4.6
D2-a	C/dune	-13	6.8	28.9	20.7	27.1	84	13.6	1.3	0.1	15	1.3
D2-b	C/dune	-28	25.0	30.8	13.4	18.7	88	9.8	1.1	0.1	11	1.1
D2-c	C/dune	57-59	7.1	27.1	30.1	29.1	94	4.7	0.1	0.3	5	1.4
D2-d	2C	61-71	1.0	4.2	5.7	41.1	52	39.2	5.1	0.9	45	2.7
D2-e	3AhC	-81	0.1	1.0	5.5	44.6	51	41.7	4.1	0.7	46	2.3
D2-f	4Ahb1	-96	0.0	0.6	4.2	41.4	46	43.0	5.1	0.8	49	4.8
D2-g	4Ahb2	-112	0.0	0.5	4.9	47.7	53	39.0	4.3	0.8	44	2.8
D2-h	4Ahb3	112+	0.0	0.4	1.5	31.1	33	56.1	5.7	2.0	64	3.1
D3-a	C/dune	-12	23.3	41.6	11.3	12.0	88	9.9	0.7	0.4	11	0.9
D3-b	2C	-17	0.9	2.2	3.9	34.5	41	46.6	8.0	0.8	55	3.1
D3-c	3AhC	-22	0.1	0.6	4.3	40.6	45	42.9	7.3	0.7	51	3.7
D3-d	4Ahb1	-32	0.5	0.9	4.9	42.4	49	40.0	7.5	0.8	48	3.0
D3-e	4Ahb2	-35	0.0	0.2	3.2	43.6	47	45.3	6.5	0.8	53	0.3
D3-f	4Ahb3	-39	2.2	3.3	2.9	26.4	35	50.8	11.8	1.5	64	1.1
D3-g	4Ahb4	40+	18.1	27.6	12.8	15.5	74	14.0	7.3	2.2	24	2.5

No.	Site description	Aspect	Inclination [°]	Width [m]	Length [m]	Depth [cm]
1	Slope	SE	13	18	10-14	65
2	Crest, bowl-shaped	SE	9	1.80	3	45
3	Upper slope range, strongly wind exposed	E-SE	11	4	8	50
4	Steep slope, strongly wind exposed	S	11	2.50-25	3-10	70
5	Steep slope, vegetated bowl, more wind protected	S	19	2.50	7.50	64
6	Almost hilltop, partly vegetated	S	8	3.10	7.20	52
7	Moraine	S-SE	9	6	7	32
8	Bouldery	SE	9	36	24	50
9	Moraine	S-SE	8	27	23	35
10	Moraine, aeolian blow-outs in luv and lee	E-SE	7	7	6	43
11	Moraine	SE	12	20	200	40
12	Moraine in dunefield, barren of vegetation	SE	13	4	8.30	70
13	Moraine in dunefield	S-SE	8	25	75	80
14	Moraine in dunefield	S-SE	13	6.10	10.60	95
15	Moraine in dunefield, bouldery	SE	1	25	190	60
16	Moraine in dunefield	SE	7	8-15	20	55